



CHALMERS
UNIVERSITY OF TECHNOLOGY

Online model adaptation for optimal control of HEVs

Master's thesis in Systems, control & mechatronics

GINA BJELKENSTEDT

MASTER'S THESIS EX046:2018

Online model adaptation for optimal control of HEVs

GINA BJELKENSTEDT



CHALMERS
UNIVERSITY OF TECHNOLOGY

Department of Electric Engineering
Division of Systems and Control
Research group of Mechatronics
CHALMERS UNIVERSITY OF TECHNOLOGY
Gothenburg, Sweden 2018

Online model adaptation for optimal control of HEVs
GINA BJELKENSTEDT

© GINA BJELKENSTEDT, 2018.

Supervisor: Martin Sivertsson & Chih Feng Lee, Volvo Cars Corporation
Examiner: Nikolce Murgovski, Chalmers University of Technology

Master's Thesis EX046:2018
Department of Electrical Engineering
Division of Systems and Control
Research group of Mechatronics
Chalmers University of Technology
SE-412 96 Gothenburg
Telephone +46 31 772 1000

Typeset in L^AT_EX
Gothenburg, Sweden 2018

Online model adaptation for optimal control of HEVs
GINA BJELKENSTEDT
Department of Electrical Engineering
Chalmers University of Technology

Abstract

The thesis explores the concept of online model adaptation and its benefit in optimal control of hybrid electric vehicles (HEVs). An algorithm is proposed for online adaptation of power losses of the internal combustion engine, the integrated starter generator and the electric rear axle drive, subject to constraint on demanded convexity with respect to delivered power. It is shown that the algorithm can be formulated as a convex quadratic program that can be solved with existing solvers.

The total system performance is evaluated by applying the well-known Equivalent Consumption Minimization Strategy (ECMS) for minimizing fuel consumption over a prediction horizon. It is shown that the model adaption is able to compensate for the neglected system dynamics in the control model, thus decreasing fuel consumption, while sustaining target battery charge to its initial value.

Keywords: hybrid electric vehicle, optimal control, model adaptation, look-up tables, least square criterion, data fitting

Acknowledgements

Firstly, I would like to thank Martin Sivertsson and Volvo Cars Corporation for the opportunity and experiences during the thesis. Also, thank you to Chih Feng Lee at Volvo Cars for helping out and urging me to write in order to finish my thesis.

Secondly, I would like to thank Nikolce Murgovski at the department of Electrical Engineering at Chalmers University of Technology for his support and guidance during the thesis.

Finally, thank you to my family and friends for sticking around through it all.

Gina Bjelkenstedt, Gothenburg, June 2018

Contents

List of Figures	xi
List of Tables	xv
1 Introduction	1
1.1 Background	1
1.2 Purpose	2
1.3 Related work	2
1.4 Outline	3
2 System overview	5
2.1 The Hybrid Electric Vehicle	5
2.1.1 Architecture of studied hybrid powertrain	7
2.2 Energy Management of Hybrid Electric Vehicles	8
2.2.1 Equivalent consumption minimization strategy, ECMS	8
3 System modeling	9
3.1 Vehicle longitudinal dynamics	9
3.2 Battery model	10
3.3 Powertrain components and losses	11
3.3.1 Electric machines	12
3.3.2 Internal combustion engine	13
3.4 Look-up tables	13
3.4.1 Piece-wise linear approximations	14
3.4.2 Mapping component losses	15
3.5 ECMS formulation	17
4 Problem description	19
4.1 Optimization problem	20
5 Method	23
5.1 Baseline model and measurements	23
5.2 Model adaptation	25
5.2.1 Handling of data and key parameters	26
5.2.2 Initialization and parameter adaptation	28
5.2.3 Overview of the adaptive approach	30
5.3 Integration with ECMS-solver	30

5.4	Standard QP-formulation	33
6	Results	35
6.1	Model error and accuracy	35
6.1.1	Electric machines	35
6.1.2	Internal combustion engine	40
6.2	Impact on fuel consumption	43
7	Conclusion and Future Work	47

List of Figures

2.1	Different powertrain configurations for HEVs.	7
2.2	Illustration of studied hybrid powertrain architecture, a parallel configuration with an added electric rear axle drive.	7
3.1	Equivalent circuit for modeling the battery where U_{oc} is the open circuit voltage, I_b is the current of the battery, R_i is the internal resistance of the battery and U_b is the voltage of the battery.	11
3.2	Piece-wise linear approximation of a function $f(x)$ where $n_k = 7$. The solid blue line represents the function being approximated and the dashed red line the approximation. Grid-points are marked with red circles.	14
3.3	Finding the normalized offset α for the current operating speed ω related to the table after first finding the interval in which ω is located. 16	
3.4	Interpolated model for $\omega(t) = 120$ rad/s shown with a dashed black line with circles marking break-points using look-up tables. The normalized offset $\alpha = 0.29$ while the model for ω_i and ω_{i+1} is shown in blue and red respectively.	16
4.1	Generic look-up table structure related to an actuator. Dimensions are given by the number of knot points that in turn defines the grid from which models for a given operating point can be derived by interpolation.	19
5.1	Model error for the ISG over a data set. Measurements are shown in blue and baseline estimation in red.	24
5.2	Model error for the ERAD over a data set. Measurements are shown in blue and baseline estimation in red.	24
5.3	Model error for the ICE over a data set. Measurements are shown in blue and baseline estimation in red.	25
5.4	Schematic of storing and handling of new data. After the limit is reached (five in this example) new data is added while the oldest data is removed. Only data points that passes the criteria will be added.	26
5.5	Finding key parameters, ie optimization variables, in stored data. In this example two optimization variables are identified where in the current set of stored data and will be estimated to reduce the model error.	27

5.6	Example of how available data is used to find the key parameters. In the left matrix it is seen that there is data scattered over two different speeds, ω_5 and ω_6 , in four and two different cells of respective speed. When an excitation limit of 75 data samples is applied this reduces and the key parameters can be identified in the right matrix.	28
5.7	Data fitting over current available data from n_0 to n_f for the ISG and ICE respectively. Data is marked with blue circles, the baseline model with solid black lines and the newly fitted model with dashed red lines.	29
5.8	Illustration for Case 1-3, where different models may be used either for ECMS or fuel consumption calculations. No adaptation occurs, all models are fixed during simulation. Inputs are the drive cycle, initial SOC and final SOC. Output is the fuel consumption. The plant represents the actual vehicle and T^* is the optimal torque found by the ECMS.	31
5.9	Illustration for Case 4 where the model used for ECMS is updated based on model error. Inputs are the drive cycle, initial SOC and final SOC. Output is the fuel consumption. The plant represents the actual vehicle and T^* is the optimal torque found by the ECMS. . . .	32
6.1	Powerlosses in the ISG. Measured values are shown with blue, estimated values using the baseline model are shown in red and estimated values using an adaptive model are shown in yellow. It can be seen that the model error of the adaptive model decreases compared to the baseline model with regards to the measurements.	36
6.2	Observations from using the adaptive approach over the given data set in the ISG. A total of 15 updates is performed. In the upper left figure it is seen that the adaptive model lies closer to the mean value of the measurement data compared to the baseline model. The upper right picture shows that the cumulative error gradually decreases compared to the baseline model. The bottom left picture shows how the adaptive model have a lower RMSE and the bottom right picture shows at which samples the update was performed.	37
6.3	Identified key parameters for the ISG over the given data set when using the adaptive approach. Here a total of 7 unique points was used during optimization.	37
6.4	Comparison of baseline model and the current model of the ISG after the final update created by performing continuous optimization to minimize model error. The fitted model using the adapted approach is shown in dashed red lines and the baseline model is shown in black.	38
6.5	Powerlosses in the ERAD. Measured values are shown with blue, estimated values using the baseline model are shown in red and estimated values using an adaptive model are shown in yellow. The model error of the adaptive model decreases compared to the baseline model with regards to the measurements.	39

6.6	Observations from using the adaptive approach over the given data set in the ERAD. A total of six updates is performed. The upper left figure shows the adaptive model is closer to the mean value of the measurement data compared to the baseline model. The upper right picture shows the cumulative error gradually decreasing compared to the baseline model. The bottom left picture shows how the adaptive model have a lower RMSE and the bottom right picture shows at which samples the update was performed.	39
6.7	Identified key parameters for the ERAD over the given data set when using the adaptive approach. Here a total of two unique points was used during optimization.	40
6.8	Comparison of baseline model and the current model of the ERAD after the final update created by performing continuous optimization to minimize model error. The fitted model using the adapted approach is shown in dashed red lines and the baseline model is shown in black.	40
6.9	Powerlosses in the ICE. Measured values are shown with blue, estimated values using the baseline model are shown in red and estimated values using an adaptive model are shown in yellow. The adaptive model approaches a smaller model error compared to the baseline model as data become available.	41
6.10	Observations from using the adaptive approach over the given data set of the ICE. A total of 45 updates is performed. In the upper left figure it is seen that the adaptive model over most intervals lies closer to the mean value of the measurement data compared to the baseline model. The upper right picture shows that the cumulative error is smaller compared to the baseline model. The bottom left picture shows how the adaptive model has a lower RMSE and the bottom right picture shows at which samples the update was performed.	42
6.11	Identified key parameters for the ICE over the given data set when using the adaptive approach. A total of 7 unique points was adapted during optimization over four different speeds.	42
6.12	Comparison of baseline model and the current model of the ICE after the final update created by performing continuous optimization to minimize model error. The fitted model using the adapted approach is shown in dashed red lines and the baseline model is shown in black.	43
6.13	Driving cycles used for system performance evaluation.	43
6.14	Powerloss estimations during the FTP-75 driving cycle using the baseline model and correct model. The upper picture shows powerloss for the ISG while the bottom picture shows powerloss for the ICE.	44
6.15	Powerloss estimations during the WLTC driving cycle using the baseline model and correct model. The upper picture shows powerloss for the ISG while the bottom picture shows powerloss for the ICE.	44
6.16	State of charge trajectories and fuel consumption of the FTP-75 cycle for simulations using the baseline and adaptive model respectively during ECMS.	45

6.17 State of charge trajectories and fuel consumption of the WLTC cycle for simulations using the baseline and adaptive model respectively during ECMS.	45
--	----

List of Tables

3.1	Number of grid-points, n_{gp} , in the look-up tables of powerlosses for different actuators.	15
5.1	Overview of the four different cases used for simulation of the ECMS-solver. Cases differ by which model is used during optimization of torque split and calculation of the fuel consumption.	32
6.1	Fuel consumption from simulation with a shrinking horizon using different models during ECMS in two different driving cycles.	45

1

Introduction

This chapter presents a short introduction to the topic of the thesis by giving a brief background of the automotive markets today together with an overview of related research. Additionally the scope and purpose of the thesis is defined.

1.1 Background

In order to reduce the environmental impact of the automotive industry both emission and fuel efficiency requirements are tightening in markets all over the world. At the same time both battery technology and infrastructure are continuously improving which have led electrified vehicles (hybrids, plug-in and battery electric) to become both more viable and available at lower costs. Consequently the market for electrified vehicles has quickly grown over the last few years and in 2017 the global sales of new electric vehicles passed one million units [1]. While this still corresponds to a low global market share of only 1.3%, it has also been estimated that by the year of 2030 the share of sold electrified vehicles could range from 10 – 50% of new units [2]. Electrified vehicles, counting both battery and hybrid vehicles, are thus expected to gain market shares from the conventional vehicles in the future [2].

Volvo Cars is a well-known brand and manufacturer within the automotive industry and has been in operation since 1927. After 90 years of business the sales reached over 570 000 cars globally in 2017. During the same year Volvo Cars also announced that all launches from 2019 will have an electric motor [3]. Cars with pure combustion engines will gradually be phased out and be replaced by cars either enhanced with electrified options or be fully electric, thus placing electrification at the core of future business.

Following this announcement and the general trends within the industry it will be crucial to continue research and development in the field of hybrid electric vehicles and hybrid powertrains to reach new targets and a successful implementation of the electrification strategies. Many of the electrified vehicles will be hybrids electric vehicles (HEV) containing two power sources, one combustion engine and one electrical battery. However, to achieve the full potential of the HEV and reduce fuel consumption and emissions it is necessary to employ an efficient energy management since the additional power source yields the need to split the power between engine and battery.

Model based optimal control uses knowledge of the system to optimize the usage of the available actuators. As such the system is heavily reliant on the model that is used, which ideally should capture all important phenomena and behaviour accurately. Today the models are fixed from a base-calibration, thus they cannot cover changes in the ambient conditions or other effects such as vehicle to vehicle variations. A bias or undesired decrease in accuracy and performance may therefore be present with time. Online model adaptation of certain parameters could be a way to achieve a model with high accuracy for use in optimal control methods in HEVs. High accuracy should ultimately increase optimality of the resulting control scheme whereas a model with poor accuracy will instead have a negative impact. The resulting control scheme will in turn affect the total energy consumption of the vehicle.

1.2 Purpose

The purpose of the thesis is to explore the concept of online model adaptation and its possible benefits in optimal control of HEVs. This can be divided into two main parts where the first part involves investigating the accuracy of the modeled powerlosses within the powertrain. In addition to this it also involves development of an algorithm which is able to adapt these models that could potentially be used in optimal control. The components of the powertrain that will be included are the internal combustion engine, the integrated starter generator and the electric rear axle drive. The second part involves evaluating the performance and impact on the total system with regards to the fuel consumption.

The goal is to increase accuracy of the model and compensate for model errors, variations and slow unmodeled dependencies. By increasing the accuracy of the model the performance of used optimal control methods may also improve while at the same time yield the possibility to incorporate previously neglected variations.

1.3 Related work

Over the years a substantial amount of research have been made within the area of energy management and optimal control in HEVs. This includes control strategies such as dynamic programming, Pontryagin's minimum principle and equivalent-consumption minimization strategies (ECMS). The thesis will use this theory and relevant findings will be presented later on. For a more thorough introduction to the field of HEV, control and modelling the reader is referred to [4].

Regardless of the used optimization technique to perform energy management of a hybrid electric vehicle, an implementation usually requires knowledge about future driving conditions and this could prove challenging in a real-time application. However, obtaining a behaviour for a real-time controller that is as close to optimal as possible requires adaptation to varying driving conditions [5]. Two alternatives for this is to use either feedback control or model predictive control (MPC) [5]. Results

from offline optimization can however be used as benchmarks for evaluation.

Further, the problem of fitting a function to a set of data points is fundamental and have been studied for many years. This holds true also for the automotive industry where identification and adaptive estimation of parameters have been researched in several different applications. One such application is the adaptation of look-up tables. Look-up tables are a commonly used technique to approximate nonlinear relationships and operating point dependencies and consists of number of parameters which models the input-output relationship.

A number of approaches have been studied to perform online adaptation of these tables. For instance a recursive least square method with a forgetting factor is used in [6], which have been applied to a two dimensional problem in both simulation and real-time. A similar approach is used in [7] where the proposed control system was shown capable of compensating different effects such as manufacturing tolerances or wear of the engine with a relatively low computational effort.

Kalman filters is another approach that have been used to approximate look-up table parameters. For instance, in [8] adaptation in an air mass-flow sensor application is performed and [9] presents a method for updating an entire table based on information only at the current operating conditions in a battery resistance estimation application. In [10] another method using Simplified Kalman filter (SKF) is presented to estimate NO_x . The approach using SKF requires less memory and calculation resources compared to an ordinary Kalman filter approach while achieving similar accuracy. Adaptive look-up tables have also been used for identification without control application. For instance in [11] where engine friction torque is estimated using polynomial approximation.

Although there have been previous work on updating look-up tables, the parameters have been unconstrained. Thus an addition of constraints on parameter values in the tables would provide another factor that needs to be considered. However, fitting problems arise in many other areas where constraints are present. For instance, the problem of fitting convex piece-wise linear function to given data by a clustering algorithm is presented in [12]. The algorithm is based on a least-square criterion where partitioning of data and fitting are performed alternating.

1.4 Outline

The report is structured as follows: Chapter 2 provides basic concepts and configurations of a hybrid electric vehicle and energy management. The studied hybrid powertrain is also introduced. Chapter 3 then continues to define the models of the vehicle, battery and powertrain components. The common technique of using look-up tables to approximate nonlinear relationships is also presented and relates to the models used. In closing of the chapter the ECMS formulation is defined. Chapter 4 presents the general optimization problem. Chapter 5 presents used methodology

to solve the problem where an algorithm for adapting key parameters of a model is proposed. Chapter 6 presents all major findings when applying model adaptation, both from analyzing model accuracy in relation to collected measurements in a system identification perspective and also the total system performance regarding fuel consumption. Chapter 7 gives conclusions together with suggestions for further research.

2

System overview

This chapter provides an overview and necessary theory regarding the general hybrid vehicle. Energy management of hybrid electric vehicles is also presented.

2.1 The Hybrid Electric Vehicle

In a conventional vehicle the mechanical power required to propel the vehicle is provided directly from an internal combustion engine, ICE, as the actuator and a high-capacity fuel storage as the power source. In a hybrid electric vehicle an additional power source and actuator is equipped as a complement. The new components usually consists of a rechargeable electrochemical battery as a power source and at least one electric motor as the actuator. Hence the definition of a hybrid as this type of vehicle is able to combine two different propulsion alternatives. This in turn creates an extra degree of freedom compared to the conventional vehicles since the HEV offer a selection of which power source or actuator to use in order to fulfill the request of the driver.

With the addition of electric components in the propulsion system new possibilities to reduce the fuel consumption is introduced. The battery can be used as an energy storage buffer and also allow regenerative braking where parts of the kinetic energy in the vehicle can be recovered and stored as electrical energy for later use. A hybrid propulsion system can also avoid operating in low efficiency regions of the ICE by providing some of the demanded torque during short accelerations or even shut down the ICE during idling or low speeds. As a consequence the combustion engine can be downsized to a smaller and less powerful engine since the power demand can be split over two power sources leading the engine able to operate at a better average efficiency [4].

Hybrid electrical vehicles can be classified with different characteristics of hybridization ranging from a micro hybrid to a plug-in hybrid, PHEV, before reaching a fully electric vehicle.

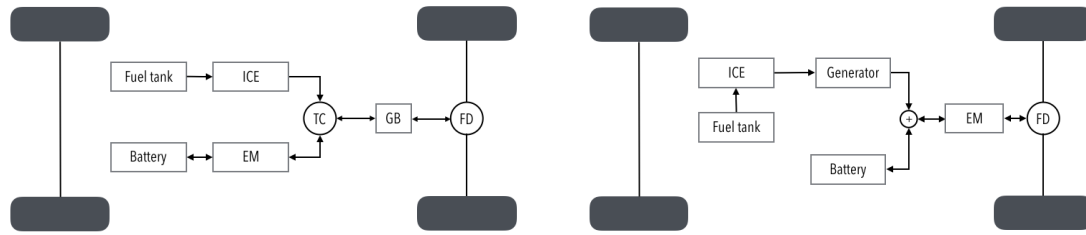
1. Conventional vehicle: ICE is the only source of power.
2. Micro hybrid: Allows the ICE to shut down and restart to reduce time in idling in non electric vehicles. Mainly used with heuristics.
3. Mild hybrid: The ICE is usually coupled with the electric machine which allows the engine to be turned off when coasting, stopping etc. Regenerative

breaking and some power assist to the engine can be used but no pure electric propulsion only is possible. Mainly used with heuristics.

4. Full hybrid: Shares the same characteristics as a mild hybrid but can run either on engine, battery or a combination of both. Instead of heuristics an energy management strategy is used to minimize fuel consumption by coordinating the actuators.
5. Plug-in hybrid: Shares the same characteristics as a full hybrid but can restore battery fully by connecting to an external power grid.
6. Electric vehicle: Propulsion only uses electric motors powered by a battery rechargeable from a power grid or a hydrogen fuel cell.

In addition to this classification there exist three main types of powertrain architectures for the full or plug-in hybrids, each with its own advantages and disadvantages [13]:

- Parallel - vehicles of this type can use both the engine and the electric motor simultaneously for propulsion as they are both mechanically linked to the wheels. In a parallel hybrid the battery can also be recharged with regenerative braking or from the engine if the power demand of the vehicle is low. The engine may be downsized compared to a conventional vehicle but the engine cannot operate in the most efficient conditions as it must be able to span over a wide range. A schematic of a parallel powertrain configuration is illustrated in Figure 2.1a.
- Series - this type of hybrid only uses the electric motor for propulsion where the power is provided from either a battery or an engine and generator set-up. Compared to the parallel hybrid architecture the series hybrid can operate in the most efficient conditions as the engine is only used for recharging the battery. However, in the conversion from engine power to electric power there still exist inefficiencies which the parallel hybrid does not have. This type usually requires a larger battery and motor than a parallel hybrid but also comes with a simpler drivetrain as the need for transmission is eliminated. As in the parallel hybrid the battery can be charged either with regenerative braking or from the engine. A schematic of a series powertrain configuration is illustrated in Figure 2.1b.
- Combined or power-split - combines the parallel and series architectures.



(a) Parallel HEV configuration consisting of a fuel tank, combustion engine, battery, electric motor (EM), torque converter (TC), gearbox (GB) and drive transmission (FD).
 (b) Series HEV configuration consisting of a fuel tank, combustion engine, generator, battery, electric motor (EM) and drive transmission (FD).

Figure 2.1: Different powertrain configurations for HEVs.

2.1.1 Architecture of studied hybrid powertrain

The architecture of the studied powertrain is defined by the Scalable Product Architecture (SPA) developed at Volvo Cars. The SPA platform is modular and based on a parallel hybrid configuration with the addition of an electric rear axle drive (ERAD) to the rear axle together with a one speed gearbox (EGB). Other main components of the configuration includes the internal combustion engine (ICE), fuel tank, battery, integrated starter engine (ISG), eight-speed gearbox (GB) and a final drive transmission (FD). An illustration of the configuration is presented in Figure 2.2.

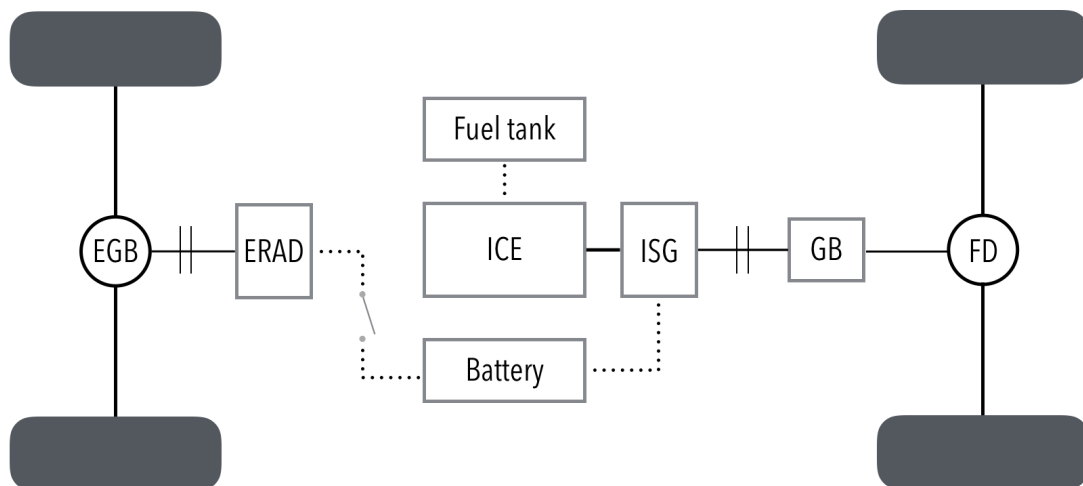


Figure 2.2: Illustration of studied hybrid powertrain architecture, a parallel configuration with an added electric rear axle drive.

It should be noticed that the ISG is coupled with the drive shaft and thereby me-

chanically linked to the ICE. As such it is not possible to run the ISG individually and for an all electric drive the ERAD can be used. The coupling between ISG and ICE does however enable charging of the battery from the ICE while running both ISG and ICE.

2.2 Energy Management of Hybrid Electric Vehicles

Hybrid electric vehicles have quickly emerged as a way to reduce fuel consumption. However, the improvements are highly dependent on the energy management strategy and control of the power split [4]. With the extra degree of freedom in hybrid electric vehicles created by adding new components this also creates a need to determine how much power is to be supplied and from what power source in the most efficient way. This is referred to as energy management strategies or EMS.

2.2.1 Equivalent consumption minimization strategy, ECMS

Equivalent consumption minimization strategy, ECMS, is a real-time approach [5] often used within the area of optimal control in hybrid electric vehicles. The intention is to reduce a global optimization problem by rewriting it as an instantaneous minimization based on actual energy in the powertrain instead [4]. The control strategies then aims to minimize the fuel consumption of the vehicle.

Pontryagin's minimum principle, PMP, provides a set of necessary conditions required for optimal control [14] and introduces a function to minimize called the Hamiltonian. The Hamiltonian is defined as

$$H(x(t), \lambda(t), u(t), t) = V(x(t), u(t), t) + \lambda(t)f(x(t), u(t), t) \quad (2.1)$$

where $x(t)$ is the state variable, $\lambda(t)$ is the costate variable and $u(t)$ is the control or input variable. Applying a power based formulation [4] the Hamiltonian can then be expressed as

$$H = P_f(t) + \lambda(t) \cdot P_{ech}(t) \quad (2.2)$$

where P_f is the fuel power, P_{ech} is the electrochemical power from the battery and the costate λ acts as a equivalence factor to convert battery power to be comparable to the fuel power. The optimal value of λ will be dependent of the driving cycle and the value will also have impact on the depletion of the battery.

3

System modeling

Development of new functions and performing simulations of vehicles or vehicle behaviour requires models of the various components and systems. The purpose of creating models of the systems and components within the vehicle are in this case to reproduce the energy flow which provides a way to estimate fuel consumption and vehicle states.

A conventional vehicle may be modeled using two main elements representing vehicle longitudinal dynamics and powertrain dynamics that includes only a combustion engine. For a hybrid electric vehicle as in this case, additional components including the battery also need to be modeled. Each system or component may also contain sub-systems modeled in different ways depending on technical or computational requirements.

3.1 Vehicle longitudinal dynamics

The vehicle longitudinal dynamics [4], consists of four elements representing traction forces, rolling resistance forces, aerodynamic drag forces and gravitational forces as

$$m_v \frac{d}{dt} v_v = F_{inertia} = F_{trac} - (F_{roll} + F_{aero} + F_{grav}) \quad (3.1)$$

where m_v is vehicle mass, v_v is vehicle speed and thus it follows that $\frac{d}{dt} v_v = a_v$ is the acceleration.

$$F_{roll} = (c_{r0} + c_{r1} v_v) m_v g \cos(\delta) \quad (3.2)$$

$$F_{aero} = \frac{1}{2} \rho_{air} A_f c_d v_v^2 \quad (3.3)$$

$$F_{grav} = m_v g \sin(\delta). \quad (3.4)$$

The rolling force due to resistance at the tires can be expressed by (3.2) where g is the gravitational acceleration, δ is the inclination of the road and both c_{r0} and c_{r1} are coefficients which defines an affine function dependent on the vehicle speed v_v . Aerodynamic drag is expressed by (3.3) where ρ_{air} is the density of the air, A_f is

the frontal area of the vehicle and c_d is the aerodynamic drag coefficient. Finally the gravitation will effect the vehicle according to (3.4).

Using a backward approach where speed is used as input and the engine torque together with the fuel consumption are outputs the tractive force required by the powertrain to propel the vehicle can then be found by rearranging equation (3.1) and yields

$$F_{trac} = F_{inertia} + F_{roll} + F_{aero} + F_{grav}. \quad (3.5)$$

$F_{inertia}$ is positive when the vehicle is accelerating and negative during deceleration, whereas F_{grav} is positive when driving uphill and negative when going downhill. The required torque at the wheels is then given by

$$T_{req,wh} = F_{trac} + r_{wh}(F_{roll} + F_{aero} + F_{grav}) \quad (3.6)$$

where r_{wh} is the radius of the wheels. Equation (3.6) can also be expressed in term of powers by multiplying all terms with the rotational speed at the wheels as

$$P_{req,wh} = T_{req,wh} \cdot \omega_{wh}, \quad (3.7)$$

where ω_{wh} is the vehicle speed, v , divided by radius of the wheel, as $\omega_{wh} = v/r_{wh}$. Since the rear and front axles are equipped with separate actuators the total wheel torque and power will be the sum of two terms as

$$P_{req,wh} = P_{req,front} + P_{req,rear}. \quad (3.8)$$

3.2 Battery model

Compared to other subsystems in a HEV, the battery is the most complicated to model since the main variables such as state of charge (SOC), voltage and current typically are related non-linearly [4]. A common approach is to use a simplified model where the voltage dynamics are neglected and the SOC is the only dynamic state.

An equivalent circuit, as shown in Figure 3.1, is introduced as a simplified model where the circuit equation can be written as a function of the battery power yielding

$$P_b(t) = U_b(t)I_b(t), \quad (3.9)$$

where I_b is the battery current and U_b is the output voltage from the battery given by Kirchoffs law as

$$U_b(t) = U_{oc}(t) - I_b(t)R_i(t) \quad (3.10)$$

where U_{oc} is the open circuit voltage and R_i is the internal resistance of the battery. Assuming U_{oc} and R_i to have a small dependency of the SOC these can be considered

constants and by combining (3.9) and (3.10) an expression for the current as a function of battery power can thus be defined as

$$I_b(t) = \frac{U_{oc}(t) - \sqrt{U_{oc}^2(t) - 4R_b(t)P_b(t)}}{2R_i(t)}. \quad (3.11)$$

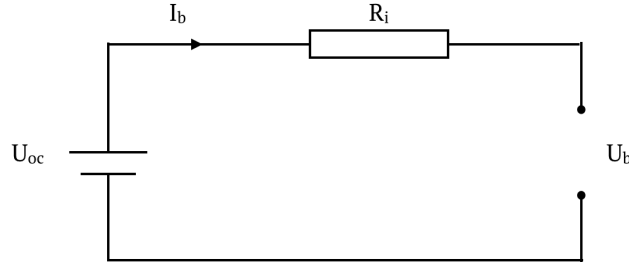


Figure 3.1: Equivalent circuit for modeling the battery where U_{oc} is the open circuit voltage, I_b is the current of the battery, R_i is the internal resistance of the battery and U_b is the voltage of the battery.

The SOC, $\xi(t)$, is defined as the ratio

$$\xi(t) = \frac{Q(t)}{Q_{nom}}, \quad \xi \in [0, 1]. \quad (3.12)$$

where $Q(t)$ is the electrical charge currently stored in the battery and Q_{nom} is the nominal charge. Thus a value of $\xi = 1$ corresponds to a fully charged battery and $\xi = 0$ to an empty battery. The dynamics of the SOC, $\dot{\xi}(t)$, are given by

$$\dot{\xi}(t) = -\frac{I_b(t)}{Q_{max}} \quad (3.13)$$

and utilizing a quasistatic approach where I_b is considered constant in during each time interval the change in SOC can be estimated as

$$\Delta\xi(t) = -\frac{I_b(t)}{Q_{max}} \Delta t. \quad (3.14)$$

From (3.11) and (3.14) it is then possible to estimate change in SOC.

3.3 Powertrain components and losses

As previously established in section 2.1.1 the current hybrid powertrain is equipped with two sources of power which can be used to propel the vehicle. However, due to losses within the powertrain the amount of energy produced at the wheels is less than the amount of energy supplied to the vehicle from its power source. For instance conversion losses can occur when power is transformed from chemical to mechanical or the other way around. Friction losses when the power flows through

different connections or other inefficiencies within the system may also contribute to the reduction of power at the wheel output.

The main components that will be investigated during the thesis will be the integrated starter generator, the electric rear axle drive, and the internal combustion engine. Collecting measurements during vehicle operation provides a way to calculate the actual losses within the powertrain which can then be used for comparison with estimated losses based on powertrain models for specific operating conditions.

3.3.1 Electric machines

There are two electric machines in the current powertrain, the ISG and the ERAD. Both can be modeled using the same relationships although they are used differently during vehicle propulsion. The ISG is mounted on the crankshaft and can act both as a start motor and as a generator to recover kinetic energy to the battery during vehicle retardation to decrease energy consumption.

$$P_{ech, isg} = U_{isg} \cdot I_{isg} \quad (3.15)$$

$$P_{mech, isg} = T_{isg} \cdot \omega_{isg} \quad (3.16)$$

$$P_{tot, isg} = P_{mech, isg} + P_{loss, isg} \quad (3.17)$$

$$P_{loss, isg} = P_{ech, isg} - P_{mech, isg} \quad (3.18)$$

The electrochemical power for the ISG is (3.15) where U_{isg} is the voltage and I_{isg} is the current. Due to losses within the powertrain the power that is delivered and used by the actuator will not be equivalent with the electrochemical power from the battery. Instead the power delivered and used by the actuators will be denoted with the subscript *mech* and is calculated by multiplying the torque and rotational speed as in (3.16) where T_{isg} is the torque of the ISG and ω_{isg} is the rotational speed of the ISG. Thus the total electrochemical power in (3.15) will correspond to the sum of the power actually used by the component, $P_{mech, isg}$, and the losses in the current operating conditions, $P_{loss, isg}$, which can also be modeled by the relation in (3.17). From (3.15)-(3.17) the power loss in each instant can be calculated from measurements as in (3.18).

For the other electric motor, the ERAD, the same relationships will hold and thus the component can be modeled as follows

$$P_{ech, erad} = U_{erad} \cdot I_{erad} \quad (3.19)$$

$$P_{mech, erad} = T_{erad} \cdot \omega_{erad} \quad (3.20)$$

$$P_{tot, erad} = P_{mech, erad} + P_{loss, erad} \quad (3.21)$$

where as previously U_{erad} is the voltage, I_{erad} is the current, T_{erad} is the torque, ω_{erad} is the rotational speed and $P_{tot,erad}$ corresponds to the total electrochemical power of the component. Finally the losses of the ERAD in each instant can be calculated again as

$$P_{loss,erad} = P_{ech,erad} - P_{mech,erad}. \quad (3.22)$$

3.3.2 Internal combustion engine

In the same way as for the electric machines the power of the internal combustion engine is calculated by multiplying torque with rotational speed thus giving

$$P_{mech,ice} = T_{ice} \cdot \omega_{ice}. \quad (3.23)$$

Further the total fuel power is modeled as the sum of the torque delivered and used by the actuators denoted and the power losses as

$$P_{tot,ice} = P_{mech,ice} + P_{loss,ice}. \quad (3.24)$$

The fuel flow rate \dot{m}_f in the engine can be expressed as a power equivalent by using the lower heating value Q_{LHV} as

$$P_{f,ice} = \dot{m}_f \cdot Q_{LHV}. \quad (3.25)$$

The lower heating value used is $Q_{LHV} = 45 \cdot 10^3$ kJ/g which converts the fuel rate from g/s to J/s, i.e. power expressed in watts. By combining (3.23) and (3.24) with the relation in (3.25) the measured losses can then be calculated from data using the following equation

$$P_{loss,meas} = P_{f,ice} - P_{mech,ice}. \quad (3.26)$$

3.4 Look-up tables

Within the automotive industry a common technique to model the kind of losses highlighted in section 3.3 is by using look-up tables [6], sometimes also referred to as maps. These are usually designed using a grid-based approach in order to be valid over large operating regions and values of the losses are provided as a function of the operating conditions. The tables are in general generated by conducting experiments where the components reach a steady-state operating condition and collecting measurements of power input and output at these points. Hence the table values will be fixed and can not account for any changes within the vehicle structures or ambient conditions. Although the process of obtaining such tables can be time consuming and tedious the main benefits of using look-up tables is the creation of a simple model which later can be evaluated quickly in the engine control unit, ECU.

3.4.1 Piece-wise linear approximations

In addition to modeling the losses as a function of operating conditions the complexity of the model can be kept low by using a piece-wise linear approximation of said function.

A function may be approximated as a piece-wise linear function over a number of sub-intervals. If $f(x)$ is a function with $x \in \mathbb{R}$ and bounded by $x \in \mathcal{D} = \{x | x_{min} \leq x \leq x_{max}\}$ the piece-wise linear approximation of $f(x)$ considering n_k sub-intervals can be expressed as

$$\hat{f}(x) = \begin{cases} a_1x + b_1, & x \in \mathcal{D}_1 \\ a_2x + b_2, & x \in \mathcal{D}_2 \\ \vdots \\ a_{n_k}x + b_{n_k}, & x \in \mathcal{D}_{n_k} \end{cases} \quad (3.27)$$

with $a, b \in \mathbb{R}$ and where the following relationship holds

$$\bigcup_{1 \leq i \leq n_k} \mathcal{D}_i = \mathcal{D} \quad \text{and} \quad \bigcap_{1 \leq i \leq n_k} \mathcal{D}_i = \emptyset$$

and the linear segments are connected on the borders of sequential \mathcal{D}_i meaning that the approximation is continuous as in Figure 3.2.

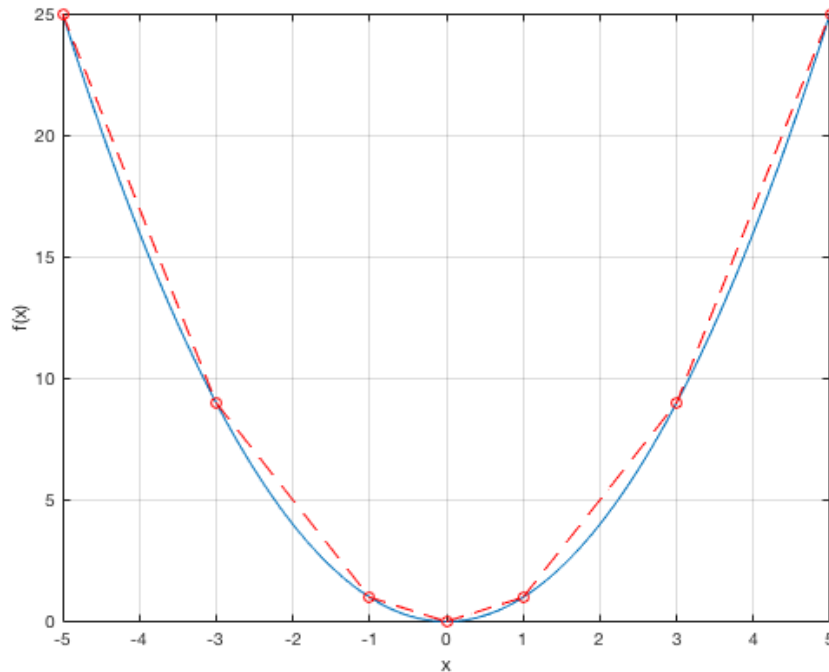


Figure 3.2: Piece-wise linear approximation of a function $f(x)$ where $n_k = 7$. The solid blue line represents the function being approximated and the dashed red line the approximation. Grid-points are marked with red circles.

One challenge with this formulation is then how to create the sub-intervals from \mathcal{D} to define a well designed grid in relation to the function that is to be approximated. In many applications it is desired to keep complexity of the models low and a trade-off will occur between achieving good accuracy and using the fewest linear parts [15], i.e. the smallest number of sub-intervals n_k . In this work however the number of sub-intervals for each model given in Table 3.1 is already considered optimal and treated as fixed while the values at the defined grid-points may be changed. Furthermore the piece-wise linear approximation in (3.27) can be expressed and obtained in a compact max-affine function form [12] as

$$\hat{f}(x) = \max_{k=1, \dots, n_k} \{a_k x + b_k\}. \quad (3.28)$$

3.4.2 Mapping component losses

The models for the ICE, ISG and ERAD respectively are seen as functions of the current operating point

$$\nu(t) = \{P_{mech}(t), \omega(t)\}, \quad (3.29)$$

where P_{mech} is defined by the torque delivered and used by the actuators and ω is the rotational speed as $P_{mech} = T_{mech} \cdot \omega$.

Each look-up table is defined by two sets of ordered points representing a number of different operating points. The size of these sets are denoted as n_ω and n_k for the number of speed and power break-points used respectively and does not need to be equi-spaced or the same for all actuators. Thus the total number of grid-points, $n_{gp} = n_\omega n_k$, may differ as presented in Table 3.1.

Table 3.1: Number of grid-points, n_{gp} , in the look-up tables of powerlosses for different actuators.

	ISG	ERAD	ICE
n_ω	16	17	28
n_k	9	9	5
n_{gp}	144	153	140

All maps are built by using two look-up tables, \mathcal{X} and \mathcal{Y} , containing values of the working power and the corresponding powerloss with respect to the grid of operating points previously defined by speed and power break-points. The first table output vector contains values of used power P_{mech} while the second table output vector are values of the powerloss P_{loss} .

For each possible speed within the limits a model can thereby be interpolated by using the original maps. This is achieved in three steps:

3. System modeling

1. Decide within what interval the current operating speed lies in relation to the tables, i.e. find the index of desired table cell by

$$i = \max\{m = 1, \dots, n_\omega \mid \omega_m \leq \omega(t)\} \quad (3.30)$$

2. Find the normalized offset $\alpha \in [0, 1]$ as in Figure 3.3 where

$$\alpha = \frac{\omega - \omega_i}{\omega_{i+1} - \omega_i}, \quad (3.31)$$

3. The interpolated output vector, i.e the model in the current operating point, is given by calculating the corresponding points (x_k, y_k) for $k \in [1, \dots, n_k]$ according to

$$\begin{aligned} X_k &= (1 - \alpha)\mathcal{X}_{(i,k)} + \alpha\mathcal{X}_{(i+1,k)} \\ Y_k &= (1 - \alpha)\mathcal{Y}_{(i,k)} + \alpha\mathcal{Y}_{(i+1,k)} \end{aligned} \quad (3.32)$$

By combining these outputs a model for the current operating speed, ω is created as in the example of Figure 3.4.

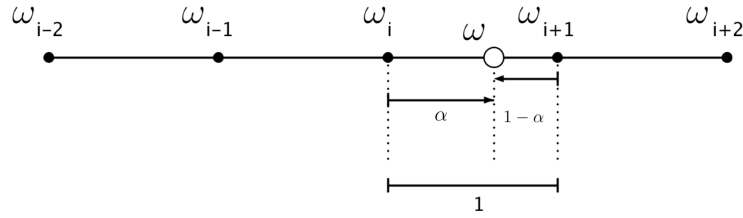


Figure 3.3: Finding the normalized offset α for the current operating speed ω related to the table after first finding the interval in which ω is located.

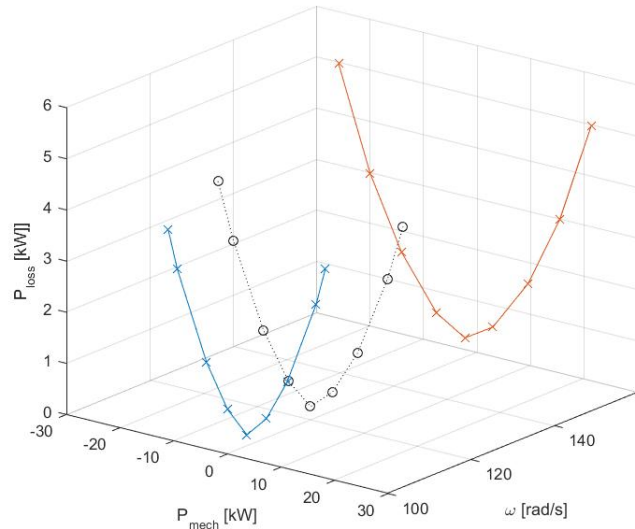


Figure 3.4: Interpolated model for $\omega(t) = 120$ rad/s shown with a dashed black line with circles marking break-points using look-up tables. The normalized offset $\alpha = 0.29$ while the model for ω_i and ω_{i+1} is shown in blue and red respectively.

3.5 ECMS formulation

Ultimately the goal of introducing ECMS in the HEV is to minimize fuel consumption. Using the Pontryagin Minimum Principle the Hamiltonian introduced in Section 2.2.1 may be rewritten in a power-based formulation.

Using the derived model of the battery as in section 3.2 the electrochemical power, i.e. effective charge or discharge, can be expressed [4] as

$$P_{ech}(t) = U_{oc}(t)I_b(t), \quad (3.33)$$

where I_b is the battery current as in (3.11) and $U_{oc}(t)$ is the open circuit voltage of the battery. Using (3.25) and (3.33) the Hamiltonian becomes

$$H = P_f(t) + \lambda(t)P_{ech}(t) \quad (3.34)$$

in which the the costate or equivalence factor $\lambda(t)$ serves as a nondimensional scaling factor in order to convert battery power to an equivalent fuel power by

$$\lambda(t) = -s(t)\frac{Q_{LHV}}{U_{oc}Q_{max}}, \quad (3.35)$$

where Q_{max} is the maximum energy stored in the battery. The objective of ECMS is to determine the torque split from the available actuators to achieve lowest possible fuel consumption. In this application there are three different choices for the torque split, thus the strategy needs to find the torques T which minimizes the Hamiltonian such that

$$\{T_{ICE,mech}, T_{ISG,mech}, T_{ERAD,mech}\} = \operatorname{argmin} H, \quad (3.36)$$

where $P_f = f(T_{ICE,mech}, \omega_{ICE})$ and $P_{ech} = f(T_{ISG,mech}, \omega_{ISG}, T_{ERAD,mech}, \omega_{ERAD})$.

Further the fuel power is modeled as

$$P_f(t) = \max\{0, P_{ICE,tot}\} \quad (3.37)$$

where in each instant the total power produced by the ICE is a sum of the useful power supplied from the actuator and the power losses as

$$P_{ICE,tot} = P_{ICE,mech} + P_{ICE,loss}. \quad (3.38)$$

The expression for the electrochemical power is instead found by combining (3.11) and (3.33) yielding

$$P_{ech}(t) = \frac{U_{oc}^2(t) - \sqrt{U_{oc}^4(t) - 4R_i(t)P_b(t)U_{oc}^2(t)}}{2R_i(t)}. \quad (3.39)$$

where the battery power, P_b , is given by

$$P_b = P_{aux} + P_{ISG,tot} + P_{ERAD,tot} \quad (3.40)$$

and the auxiliary losses, P_{aux} , is assumed constant. In the same way as in (3.38) the power for each of the electric actuators are modeled as

$$P_{ISG,tot} = P_{ISG,mech} + P_{ISG,loss}, \quad (3.41)$$

$$P_{ERAD,tot} = P_{ERAD,mech} + P_{ERAD,loss}. \quad (3.42)$$

Thereby it is evident that all three propulsion actuators are connected to a term of losses in the powertrain found in (3.38), (3.41) and (3.42). Each of these terms will thus affect the Hamiltonian (3.34) either directly or indirectly.

Additionally, the Hamiltonian to be minimized is subject to limitations in battery and actuator powers as

$$P_{b,min} \leq P_b \leq P_{b,max}, \quad (3.43)$$

$$P_{ICE,min} \leq P_{ICE} \leq P_{ICE,max}, \quad (3.44)$$

$$P_{ISG,min} \leq P_{ISG} \leq P_{ISG,max}, \quad (3.45)$$

$$P_{ERAD,min} \leq P_{ERAD} \leq P_{ERAD,max}. \quad (3.46)$$

4

Problem description

The task is to explore online adaptation of look-up tables containing data for estimating powerlosses during vehicle operation. Table outputs in each time step t is the estimated value of power loss corresponding to the current operating point $\nu(t)$ as input. The power losses are modeled using piece-wise linear functions and calculation for each output value is made by interpolation of adjacent models extracted from data stored in the look-up tables.

Each actuator in the HEV configuration described in Section 2.1.1 is connected to a term of power loss which is represented by its own model built from two connected tables. Let $\mathcal{X}^{M,m}$, $m = \{ISG, ERAD, ICE\}$, denote the original tables containing values of mechanical powers and \mathcal{Y}^M be the corresponding power losses. Dimension of both \mathcal{X}^M and \mathcal{Y}^M are given by $[n_k \times n_\omega]$ where n_k and n_ω is the number of knot points for mechanical powers and rotational speeds respectively. A visual representation of such a model with two tables is shown in Figure 4.1.

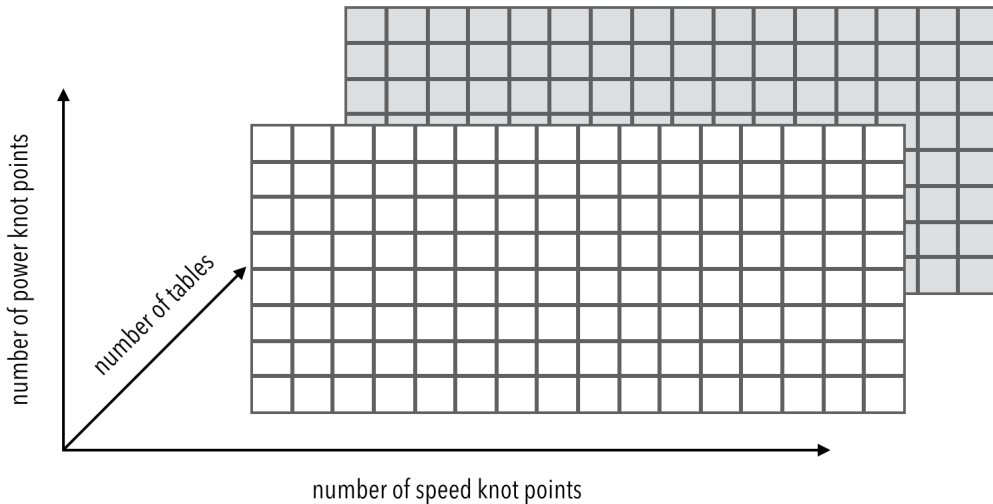


Figure 4.1: Generic look-up table structure related to an actuator. Dimensions are given by the number of knot points that in turn defines the grid from which models for a given operating point can be derived by interpolation.

Furthermore, let X_k denote the knot points and Y_k the knot values which together creates the model for the current operating point $\nu(t) = \nu_n$. Each vector has the

dimension $[1 \times n_k]$, where $x_{(k,j)}$ and $y_{(k,j)}$ denotes the j -th knot point of X_k, Y_k . Thus the interpolated model is given by (4.1) and (4.2). Both X_k and Y_k is calculated by interpolation from \mathcal{X}, \mathcal{Y} according to (3.30), (3.31) and (3.32).

$$X_k = [x_{(k,1)}, x_{(k,2)}, \dots, x_{(k,j)}] \quad j = 1, \dots, n_k, \quad (4.1)$$

$$Y_k = [y_{(k,1)}, y_{(k,2)}, \dots, y_{(k,j)}] \quad j = 1, \dots, n_k. \quad (4.2)$$

After establishing necessary notation the solution of the problem is thus to find a way to update the tables containing the data for modelling losses within the powertrain using collected measurements from the actual system compared to only using fixed tables derived from calibration performed offline as previous. Finding said solution is however non-trivial as the models and proposed algorithm should fulfill some pre-defined properties as follows:

- Convexity in all models
- Robust to measurement noise
- Low memory and computational requirements

This yields the table parameter updates to also be constrained and in order to find a solution there is two main parts that needs to be considered. The first is interpolation which defines the table outputs and the second is adaptation which defines how and when to update the tables and store data.

Here the look-up tables are represented by a number of nodes with two variables as $(\mathcal{X}_{(i,k)}, \mathcal{Y}_{(i,k)})$ for a given number of speeds $i = [1, \dots, n_\omega]$ and number of knots $k = [1, \dots, n_k]$. The output variable of the table is the estimated powerloss, \hat{y} , and values of the output between the gridded nodes are calculated by linear interpolation. From this it can be concluded that there exist multiple ways of adapting the output variable by changing the values of the variables which defines the nodes of the table. This could be achieved by adapting either \mathcal{X} or \mathcal{Y} , or both at the same time. By allowing both tables to change at the same time, the number of variables used in optimization will increase and may not be beneficial for a real-time implementation. Therefore the problem of adapting the look-up tables are reduced to the adaptation of \mathcal{Y} initially.

4.1 Optimization problem

The idea for updating the table values is based on minimizing the error between measurements and estimations, i.e adapting table values to accurately represent the current vehicle, powertrain and operating conditions. As previously presented the functions $P_{loss} = f(T, \omega)$ will be approximated using a piecewise linear function.

Thus the optimization then translates to finding the convex piecewise linear function $\hat{f} \in \mathcal{F}$ that minimizes the least-square fitting criterion between the estimated power loss, \hat{y} , and measured power loss, y , in N number of samples as

$$\min \sum_{n=1}^N (\hat{y}_n - y_n)^2 \quad (4.3)$$

$$\text{s.t. } \hat{y}_n \geq 0 \quad (4.4)$$

$$a_{n,l+1} \geq a_{n,l}, \quad (4.5)$$

where n marks the current interpolated model and $l = 1, \dots, n_k - 1$ denotes the l -th components of the model parameterization variables a_n and b_n as in (3.28). Equation (4.4) requires the estimated power loss to be positive at all times while equation (4.5) imposes convexity by restricting the slopes of the different line segments of the model.

4. Problem description

5

Method

Having a model of the system available online, i.e. while the system is operating, can in applications such as control or filtering be very useful. It can for instance be beneficial when a model is either required or used to make decisions about the state of the system or choosing the next input. The model should then incorporate observations up to the current time instant. Approaching problems in this way is usually called adaptive [16].

5.1 Baseline model and measurements

As the mathematical model of both the HEV and optimization problem has been defined, the next step is to investigate actual sets of measurement data. The measurements are collected during operation of a real vehicle and the powerloss in each instant is estimated as described in Section 3.3.1-3.3.2 and will be used as a reference for the baseline model applied to the same operating points.

$$P_{loss,em}^{meas} = P_{ech,em} - P_{mech,em} \quad (5.1)$$

$$P_{loss,em}^{baseline} = \max_{k=1,\dots,n_k} \{a_{k,em}P_{mech,em} + b_{k,em}\} \quad (5.2)$$

$$e_{loss,em} = P_{loss,em}^{baseline} - P_{loss,em}^{meas} \quad (5.3)$$

$$P_{loss,ice}^{meas} = P_{f,ice} - P_{mech,ice} \quad (5.4)$$

$$P_{loss,ice}^{baseline} = \max_{k=1,\dots,n_k} \{a_{k,ice}P_{mech,ice} + b_{k,ice}\} \quad (5.5)$$

$$e_{loss,ice} = P_{loss,ice}^{baseline} - P_{loss,ice}^{meas} \quad (5.6)$$

The baseline model is defined by the original maps, \mathcal{X}^M and \mathcal{Y}^M , for each component and the powerlosses are estimated as in (5.2) and (5.5). To analyze and compare the different approaches, the model error is introduced as

$$e = \hat{y} - y, \quad (5.7)$$

where \hat{y} represents the estimation using the baseline models and y the actual measurement. The model error will serve as a comparative measurement of accuracy

5. Method

and trends between data and models and each of the components will have a corresponding model error, (5.3) and (5.6). The subscript *em* represents the electric components, either the ISG or the ERAD.

The model error may also be evaluated using difference techniques such as calculating the root mean square error (RMSE) or the mean absolute error (MAE) as

$$\text{RMSE} = \sqrt{\frac{1}{N} \sum_{i=1}^N (\hat{y} - y)^2}, \quad (5.8)$$

$$\text{MAE} = \frac{1}{N} \sum_{i=1}^N |\hat{y} - y|, \quad (5.9)$$

where N is the number of samples. Low values of the model error would indicate that the estimated and measured powerloss are similar while higher values would instead suggest there is a higher bias. Average results for the three components are presented in Figure 5.1-5.3.

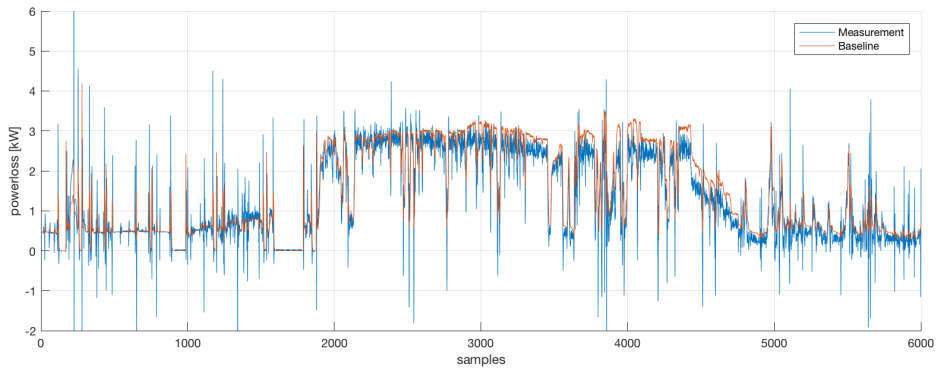


Figure 5.1: Model error for the ISG over a data set. Measurements are shown in blue and baseline estimation in red.

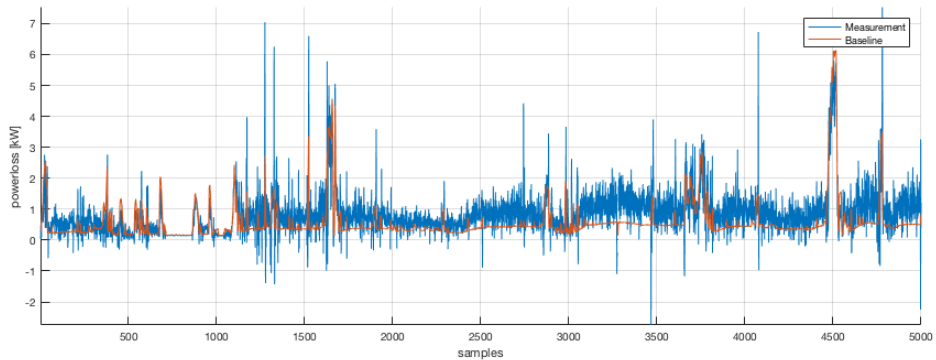


Figure 5.2: Model error for the ERAD over a data set. Measurements are shown in blue and baseline estimation in red.

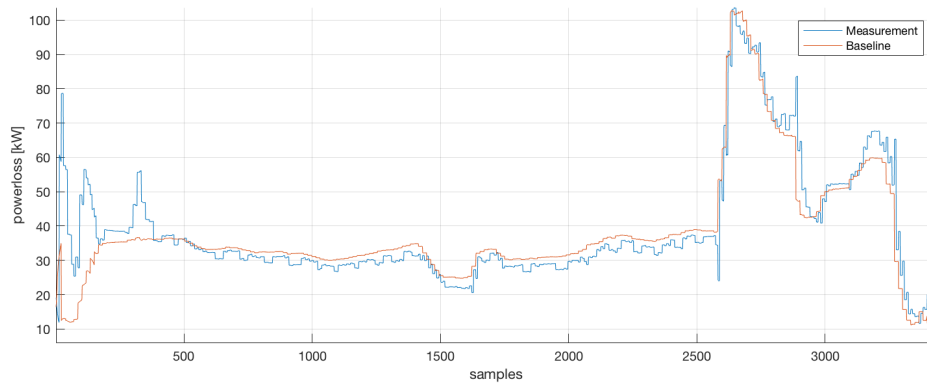


Figure 5.3: Model error for the ICE over a data set. Measurements are shown in blue and baseline estimation in red.

Typically, the baseline model estimation follows the same trends as the measurement data but there is both under- and overestimation occurring in different segments and components. Note that in some data sets the model error found could be both lower or higher than the examples shown here. However, it can be concluded that there is a model error present in all three of the components regarding powerlosses. In the electric machines the error is typically smaller compared to the combustion engine. This can be explained by the electric motors having a higher efficiency compared to the more complex behaviour of the combustion engine which also generates higher powers. The next question is then if it is possible to minimize this model error by adapting the parameters of the baseline model in order to get better estimations.

5.2 Model adaptation

With the results from previous section the baseline model is assumed to be fairly accurate but with room for improvement. However, since the baseline model is based on data covering larger operating regions it is desired for the system to remember this information and adaptation of parameters should not be performed too rapid or else useful information could potentially be lost. A trade-off will thus occur during adaptation to estimate new parameter values while at the same time using the baseline model as a reference to prevent the new estimation to rapidly deviate from the origin. Since the models and subsequently the parameters are constrained this also need to be considered during adaptation.

Development of the online parameter estimator is divided into two parts. Firstly, the data must be stored and key parameters need to be defined. To achieve a robust performance some outlier measurements may need to be discarded in order to avoid adaptation to noisy measurements. Key parameters, or optimization variables, are defined as the parameters that is connected to a certain number of data points yielding enough information to make a new estimation of parameters and fit to reduce the model error. Finding the new estimate of parameters is also the second part of the algorithm where the optimization problem is solved with regards to constraints

and available data. The optimization problem is initialized when the cumulative model error reaches the given limit and enough data is available.

5.2.1 Handling of data and key parameters

When a measurement is available, it is first processed with respect to a number of criteria and if it passes it will be stored. Otherwise it will instantly be discarded if the criteria is not passed. In this approach the criteria is set to only allow non-negative powerlosses based on measurements. Furthermore, to avoid performing estimations using transient data points a limit on the rotational acceleration is also used. The number of stored data will also be a factor which will affect the estimation. A large number of stored data will give more information about the system while the required memory and computational time will increase and should be considered if aiming for a real-time implementation.

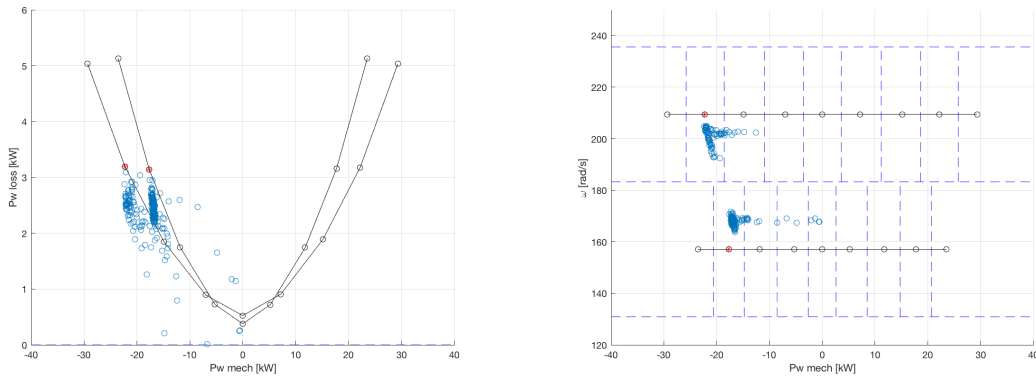
If the data point fulfills the requirements, it will be stored and added directly until the limit for the number of data stored is reached. After the limit is reached new data is added while the oldest data is removed as illustrated in Figure 5.4. By this the data used for estimation always corresponds to the latest observations and operating conditions.



Figure 5.4: Schematic of storing and handling of new data. After the limit is reached (five in this example) new data is added while the oldest data is removed. Only data points that passes the criteria will be added.

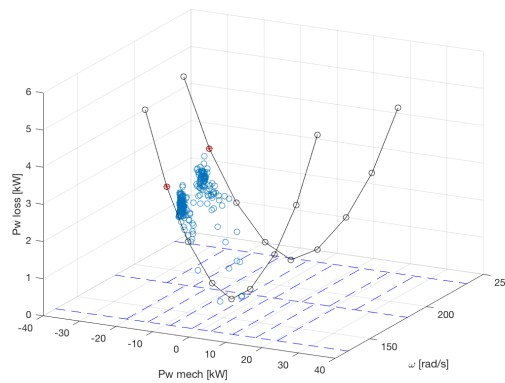
To identify key parameters based on the stored data an excitation approach is applied, meaning that there must be enough measurements within a defined distance. This clustering is performed by creating a grid over the baseline model where each cell centers the knot points of the mechanical power with respect to the rotational speed defined by the baseline model, \mathcal{X}^M . In Figure 5.5 a scenario is shown where the available data is located around two different speeds and over several grid areas. Two key parameters, $\mathcal{Y}_{5,2}$ and $\mathcal{Y}_{6,2}$, can be identified here and will be estimated to reduce the model error during optimization.

During development of the adaptation approach, another method to identify key parameters was also tested. Instead of centering the knot points in \mathcal{X} , they were used as corners which marked a small region between models. If enough data was located inside this region it was considered excited and all four knot-points defining the region was chosen as key parameters. However, when comparing the two approaches for identifying and selecting key parameters the two methods showed very similar results. Since the centered grid approach yields less used variables, typically only 1 to 2 compared to 4 to 6 in the corner region case, while achieving the same accuracy the center grid is considered more suitable in this application.



(a) Measured powerloss is shown with blue circles, the baseline model with a black line and black circles. Key parameters are shown in red stars.

(b) The grid created to center each knot points shown with blue dashed lines. Measured powerloss is shown with blue circles, the baseline model with a black line and black circles. Key parameters are shown in red stars.



(c) 3D representation of the same scenario as in 5.5a and 5.5b.

Figure 5.5: Finding key parameters, ie optimization variables, in stored data. In this example two optimization variables are identified where in the current set of stored data and will be estimated to reduce the model error.

Stored data and key parameters can also be represented using a matrix for a quick overview of the entire maps and covered operating regions as shown in Figure 5.6, illustrating the same scenario as in Figure 5.5. Each cell marks the number of data points within the corresponding gridded area. The number will increase by one every time a new data is available within the gridded area and in the same way the number will decrease by one whenever a data point is removed. In Figure 5.6 an example is shown where this approach selects two optimization variables based on the currently stored data. The left matrix shows that there is available data points scattered between several grid areas and when the excitation limit is applied only two variables are considered to contain enough information to give a reliable result.

The limit for excitation will as such be a tuning parameter for the algorithm which will affect how many model parameters are used during optimization later.

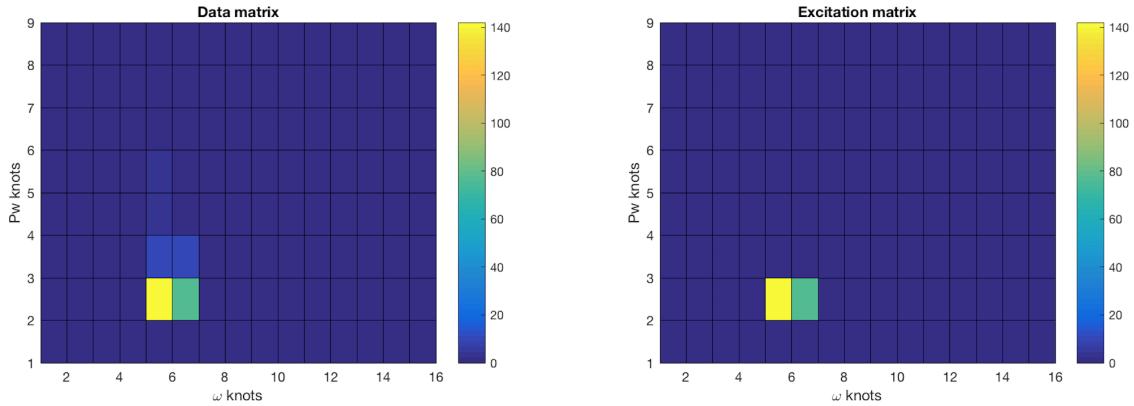


Figure 5.6: Example of how available data is used to find the key parameters. In the left matrix it is seen that there is data scattered over two different speeds, ω_5 and ω_6 , in four and two different cells of respective speed. When an excitation limit of 75 data samples is applied this reduces and the key parameters can be identified in the right matrix.

5.2.2 Initialization and parameter adaptation

Data is collected continuously and the adaptation of key parameters can be initialized either by a given time sampling or by keeping track of the cumulative model error, E , as

$$E = \sum_{n_0}^{n_f} |(\hat{y} - y)| \quad (5.10)$$

where n_0 is the first sample used and n_f is the last and current sample. If the cumulative model error reaches above a given limit while there is enough data stored, the optimization problem will be initialized. For instance, in a scenario where the model error quickly reaches $E \geq E_{lim}$ and the required data is set to 200 samples and there is only 100 samples available in the current time instant the optimization will wait and initialize once the number of stored and available data reaches 200 samples.

Parameter adaptation is then performed by solving an extended version of the general optimization problem defined in (4.3)-(4.5). This is done by rewriting previous formulation using the l_2 -norm and utilizing the vector structure of the measurements and estimations. As stated before the baseline model is based on data covering larger operating regions and it is desired to keep as much information as possible while adapting the parameters the adaptation should not be allowed to be performed too rapidly. Therefore the objective is extended to include a weighting factor μ which handles the trade-off between model error ($\hat{y}_n - y_n$) and the deviation for new values in \mathcal{Y} of the key parameters compared to the corresponding original model value \mathcal{Y}^M .

Examples of performing an optimization over a set of available data are illustrated in Figure 5.7. The extended objective function is expressed as

$$\underset{\mathcal{Y}_p}{\text{minimize}} \quad \mu \|\hat{y}_n - y_n\|_2^2 + (1 - \mu) \|\mathcal{Y}_p - \mathcal{Y}_p^M\|_2^2 \quad (5.11)$$

$$\text{s.t.} \quad \mathcal{Y}_{(i,k)} \geq 0, \quad k = 1, \dots, n_k \quad (5.12)$$

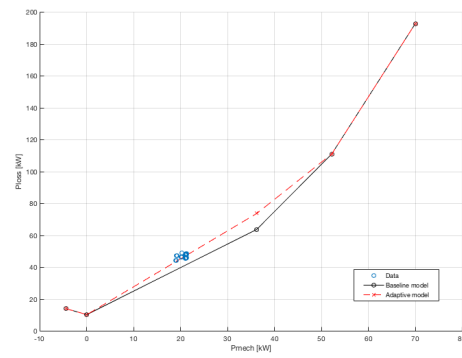
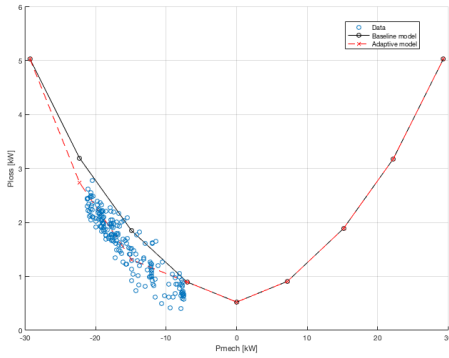
$$\frac{\mathcal{Y}_{(i,k+2)} - \mathcal{Y}_{(i,k+1)}}{\mathcal{X}_{(i,k+2)} - \mathcal{X}_{(i,k+1)}} \geq \frac{\mathcal{Y}_{(i,k+1)} - \mathcal{Y}_{(i,k)}}{\mathcal{X}_{(i,k+1)} - \mathcal{X}_{(i,k)}}, \quad k = 1, \dots, n_k - 2 \quad (5.13)$$

where index k denotes the power knot points of the speeds and index i denotes the active speeds of the key parameters involved during optimization. The length of i is defined as n_i . As before $\hat{y}_n = f(\nu_n, \mathcal{X}, \mathcal{Y})$ from (5.2) and (5.5). The variable p represents a vector containing the indices $\{i, k\}$ of the key parameters used in optimization. The length of p is thus equal to the number of key parameters. For the example in Figure 5.5 $p = [\{5, 2\}, \{6, 2\}]$. For the same example $n_i = 2$ as the model is updated in operating ranges of $i = [\omega_5, \omega_6]$. The constraints demands the powerloss model to be strictly positive and convex in relation to the delivered power. For the electric machines an additional constraint is used to ensure the minimum value of the powerloss is located at zero delivered power, given by

$$\mathcal{Y}_{(i,k)} - \mathcal{Y}_{(i,k+1)} \geq \delta_y \quad \text{if} \quad \mathcal{X}_{(i,k)} < 0, \quad k = 1, \dots, n_k \quad (5.14)$$

$$\mathcal{Y}_{(i,k+1)} - \mathcal{Y}_{(i,k)} \geq \delta_y \quad \text{if} \quad \mathcal{X}_{(i,k)} > 0, \quad k = 1, \dots, n_k, \quad (5.15)$$

where δ_y is a predefined minimum distance of the table values taken from the baseline models.



(a) Example of a data fitting over current available data for the ISG component in a case where two key parameters are used. (b) Example of a data fitting over current available data for the ICE component in a case where one key parameter is used.

Figure 5.7: Data fitting over current available data from n_0 to n_f for the ISG and ICE respectively. Data is marked with blue circles, the baseline model with solid black lines and the newly fitted model with dashed red lines.

Current implementation and solving of the optimization problem is performed using MATLAB and the nonlinear programming solver `fmincon` which finds a constrained

minimum of a function of several variables as in this case. The solver returns the new values of the key parameters that will minimize the model error according to (5.11) and the values of \mathcal{Y}_p will in the final step be updated. Once an update has occurred, the cumulative error will reset back to zero and begin tracking the model error again while using the updated map.

5.2.3 Overview of the adaptive approach

The proposed adaptive approach can be summarized as in Algorithm 1. The notation used is \mathbf{Y} and \mathbf{X} for the look-up table \mathcal{Y} and \mathcal{X} respectively, N for number of data points evaluated and E for the cumulative error. Further the measurements are denoted as ω_n, x_n and y_n for speed, mechanical power and powerloss respectively. Additionally \hat{y} is the model estimated powerloss. The algorithm alternates between handling of data and performing least-squares fit to update the identified key parameters.

Algorithm 1 Algorithm for updating look-up table parameters

Require: Initialize `storedData`, \mathbf{Y} , \mathbf{X} , E

```

1: for  $n$  in  $N$  do
2:   read  $\{\omega_n, x_n, y_n\}$ 
3:   calculate  $\hat{y}_n = f(\omega_n, x_n, \mathbf{Y}, \mathbf{X})$ 
4:   update estimation error,  $E = E + (\hat{y}_n - y_n)$ 
5:   if  $y_n \geq 0$  and  $\dot{w} \leq \dot{w}\text{Limit}$  then
6:     if number of data  $>$  dataLimit then
7:       remove oldest data point and add  $\{\omega_n, x_n, y_n\}$  to storedData
8:     else
9:       add  $\{\omega_n, x_n, y_n\}$  to storedData
10:    end if
11:  else
12:    discard  $\{\omega_n, x_n, y_n\}$ 
13:  end if
14:  if  $E >$  errorLimit and enough data in storedData then
15:    find key parameters,  $z$ , to update based on excitation in storedData
16:    minimize error between estimation and measurement over storedData
17:    store new values of  $z$  in  $\mathbf{Y}$ 
18:     $E = 0$ 
19:  end if
20: end for

```

5.3 Integration with ECMS-solver

To investigate how model adaptation will affect the total system and fuel consumption simulations are carried out using MATLAB. An ECMS-solver was provided by Volvo which is based on work from a previous master thesis [17]. The solver was then

extended to incorporate elements to calculate model error and adaptation of models.

Since the provided measurements are collected during actual vehicle operation it would require the adaptation approach to be implemented in real-time to be able to accurately make comparisons which is beyond the scope of the thesis. Instead, the measurements are used to create a new map which will represent actual vehicle operation and referred to as the correct model. This is achieved by running the adaptive approach previously presented over a number of data sets to let key parameters change according to model error between the baseline model and the measurements. Hence, there is now a baseline model and a corrected model, in which their difference will be introduced as a modelling error in simulation. The model error will not be the actual error but rather an error of the same kind that will provide information about how the solver and solutions are affected regarding fuel consumption. Additionally, during simulations only the torques of the ICE and ISG components will be optimized. The remainder of this thesis will focus on these two components.

Four cases are defined to create scenarios where different models are used to collect results. In the first case the original solver is run without extension, thus the ECMS uses the baseline model for optimization of torque split and calculation of fuel consumption. In the second case, the ECMS again uses the baseline model for optimization of torque split but instead uses the correct model to calculate the fuel consumption when there is a model error and no adaptation occurs. In the third case, the correct model is used both during ECMS and calculation of fuel consumption. Case 3 will thus provide a theoretical lower bound that corresponds to a system that operates with perfect knowledge and no model error is present. In all cases 1 to 3 the models are fixed during simulation. Figure 5.8 shows an overview of the simulation where inputs are drive cycle, initial SOC and final SOC. The output is the fuel consumption.

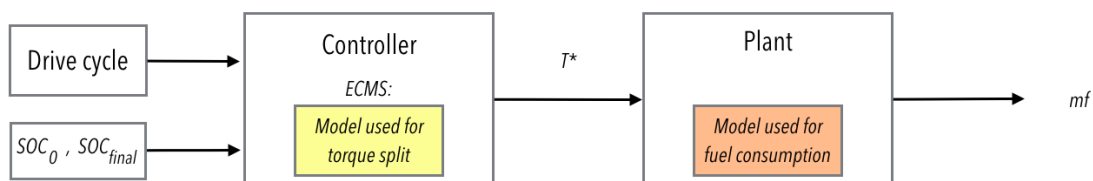


Figure 5.8: Illustration for Case 1-3, where different models may be used either for ECMS or fuel consumption calculations. No adaptation occurs, all models are fixed during simulation. Inputs are the drive cycle, initial SOC and final SOC. Output is the fuel consumption. The plant represents the actual vehicle and T^* is the optimal torque found by the ECMS.

In the fourth and last case, the ECMS starts by using the baseline model but this will be updated according to the model error estimated from the correct map. Adaptation will be performed with the same approach as when using the actual mea-

surements, the only difference lies in how the model error is defined. In simulations this is introduced as the difference between two different models rather than the baseline model and measurements. The correct model is always used to calculate fuel consumption. Figure 5.9 shows an overview of the simulation where adaptation is used. The inputs are again the drive cycle, initial SOC and final SOC while fuel consumption is the output. An overview of the different cases is presented in Table 5.1.

In the adaptive case, simulations are performed with an MPC approach where a shrinking prediction horizon is used. The horizon window is thus fixed and does not shift at each time step. Instead, the initial prediction horizon consists of the entire driving cycle and the optimal torque-split is calculated using ECMS for the horizon. Then the first step is applied and system evolution and status of SOC is observed and used as input for the next prediction horizon which is now decreased with the same length as the previous step. This scheme repeats until the end of the initial prediction horizon.

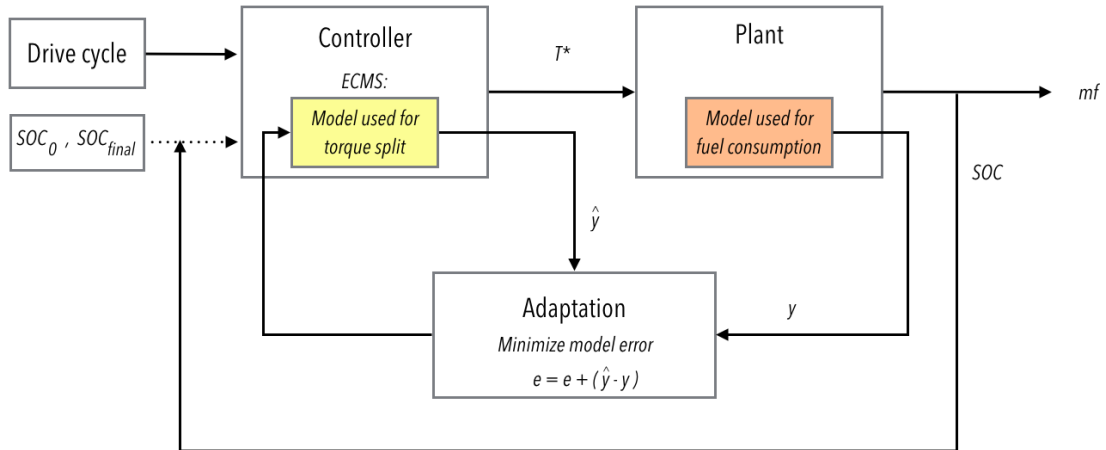


Figure 5.9: Illustration for Case 4 where the model used for ECMS is updated based on model error. Inputs are the drive cycle, initial SOC and final SOC. Output is the fuel consumption. The plant represents the actual vehicle and T^* is the optimal torque found by the ECMS.

Table 5.1: Overview of the four different cases used for simulation of the ECMS-solver. Cases differ by which model is used during optimization of torque split and calculation of the fuel consumption.

	Optimization of torque split	Calculation of fuel consumption
Case 1	Baseline model	Baseline model
Case 2	Baseline model	Correct model
Case 3	Correct model	Correct model
Case 4	Adaptive model	Correct model

5.4 Standard QP-formulation

The use of `fmincon` is suboptimal when considering a possible future real-time implementation as this is quite computationally demanding and slow. It can be shown that the optimization problem to minimize the model error can be rewritten as a quadratic programming problem in standard form. The result could be used to reduce computational time and increase efficiency of the algorithm by using another existing solver such as MATLAB `quadprog`.

The standard quadratic programming (QP) problem is formulated as

$$\min_z \frac{1}{2} z^T H z + f^T z \quad (5.16)$$

$$\text{s.t. } A z \leq b \quad (5.17)$$

$$A_{eq} z = b_{eq} \quad (5.18)$$

$$lb \leq z \leq ub \quad (5.19)$$

where z is the optimization variable and the optimization problem may be constrained by either inequality or equality constraints and bounded. Starting from the general optimization problem defined in (4.3) and introducing the notation of e for the fitting error gives

$$\min_z \sum_{n=1}^N e_n^2 = \sum_{n=1}^N (\hat{y}_n - y_n)^2 \quad (5.20)$$

$$\text{s.t. } \hat{y}_n \geq 0 \quad (5.21)$$

$$a_{n,l+1} \geq a_{n,l}, \quad (5.22)$$

where z denotes the vector of optimization variables as $z = [z_1, z_2, \dots, z_p]^T$ and p is the total number of optimization variables determined by clustering based on the set of N samples as in Section 5.2.1. Adapting the models may also involve more than one segment at a time, then the problem is extended as

$$\min_z \sum_{s=1}^S \sum_{n=1}^N e_n^2 = \sum_{s=1}^S \sum_{n=1}^N (\hat{y}_n - y_n)^2 \quad (5.23)$$

where S is the number of piecewise linear segments of the model. The same constraints are applied. Estimated powerloss at each instant, \hat{y}_n , in a segment s is given by

$$\begin{aligned} \hat{y}_n &= y_k + \frac{y_{k+1} - y_k}{x_{k+1} - x_k} (x_n - x_k) \\ &= y_k \left(1 - \frac{(x_n - x_k)}{x_{k+1} - x_k} \right) + y_{k+1} \frac{(x_n - x_k)}{x_{k+1} - x_k} \end{aligned} \quad (5.24)$$

where the term $\xi_n = (x_n - x_k)/(x_{k+1} - x_k)$ can be introduced since these values are independent of the optimization variables. The estimation will be dependent on the table of \mathcal{Y} as described in section 3.4.2 by

$$y_k = (1 - \alpha_n)\mathcal{Y}_{(i,k)} + \alpha_n\mathcal{Y}_{(i+1,k)} \quad (5.25)$$

$$y_{k+1} = (1 - \alpha_n)\mathcal{Y}_{(i,k+1)} + \alpha_n\mathcal{Y}_{(i+1,k+1)} \quad (5.26)$$

and by using equation (5.24), (5.25) and (5.26) it follows that

$$\begin{aligned} \hat{y}_n &= (1 - \xi_n)(1 - \alpha_n)\mathcal{Y}_{(i,k)} + \xi_n(1 - \alpha_n)\mathcal{Y}_{(i,k+1)} \\ &\quad + (1 - \xi_n)\alpha_n\mathcal{Y}_{(i+1,k)} + \xi_n\alpha_n\mathcal{Y}_{(i+1,k+1)}. \end{aligned} \quad (5.27)$$

From this it is evident that four different node variables are used when calculating the estimated powerloss in each instant $n \in N$. Depending on where the operating point ν_n is located the variables may not be the same for all n , i.e the indices of i and k found by clustering the data may be different. Over the entire data N the number of variables p can also vary, but in each instant limited to $p_n \in [1, 4]$.

Assuming four variables used, this can be expressed in a generic way as

$$\hat{y}_n = \phi_1 z_1 + \phi_2 z_2 + \phi_3 z_3 + \phi_4 z_4 = \Phi^T z \quad (5.28)$$

where

$$\Phi = \begin{bmatrix} \phi_1 \\ \phi_2 \\ \phi_3 \\ \phi_4 \end{bmatrix} = \begin{bmatrix} (1 - \xi_n)(1 - \alpha_n) \\ \xi_n(1 - \alpha_n) \\ (1 - \xi_n)\alpha_n \\ \xi_n\alpha_n \end{bmatrix}, \quad (5.29)$$

and

$$z = \begin{bmatrix} z_1 \\ z_2 \\ z_3 \\ z_4 \end{bmatrix} = \begin{bmatrix} \mathcal{Y}_{(i,k)} \\ \mathcal{Y}_{(i,k+1)} \\ \mathcal{Y}_{(i+1,k)} \\ \mathcal{Y}_{(i+1,k+1)} \end{bmatrix}. \quad (5.30)$$

To formulate the matrices H and f in (5.16), the fitting error in (5.20) is expanded as $e_n^2 = \hat{y}_n^2 + 2\hat{y}_n y_n - y_n^2$ from which four quadratic terms are found, yielding

$$H_\phi = \begin{bmatrix} 2\phi_1^2 & 4\phi_1\phi_2 & 4\phi_1\phi_3 & 4\phi_1\phi_4 \\ 0 & 2\phi_2^2 & 4\phi_2\phi_3 & 4\phi_2\phi_4 \\ 0 & 0 & 2\phi_3^2 & 4\phi_3\phi_4 \\ 0 & 0 & 0 & 2\phi_4^2 \end{bmatrix}, \quad f = \begin{bmatrix} 2\phi_1 y_n \\ 2\phi_2 y_n \\ 2\phi_3 y_n \\ 2\phi_4 y_n \end{bmatrix} \quad (5.31)$$

where $H = (H_\phi + H_\phi^T)/2$ to obtain a symmetric matrix.

6

Results

This chapter presents results from simulations performed in MATLAB. First the proposed algorithm is tested on the provided data collected from actual vehicle operation to evaluate model accuracy and the size of the model error. Then the total system performance regarding fuel consumption is evaluated when model adaptation is applied during different driving cycles.

6.1 Model error and accuracy

In this section, examples which represent average results when the algorithm is applied to each of the three components are presented. Accuracy and change in the system is observed using different measures such as RMSE and cumulative error.

6.1.1 Electric machines

A data set with $N = 6360$ samples is used to evaluate the ISG. Powerlosses over the entire data set and corresponding profile of ω are presented in Figure 6.1. Number of stored data used in simulation is 200 samples and the excitation limit is set to 80 data points.

A trade-off between data size and performance need to be considered. Using a lot of data will be beneficial to get stable changes of the parameters, however using more data will require more memory resources and computational time to perform data fitting. An implication of the currently used ratio between number of stored samples and excitation limit is that the maximum number of key parameters used in each optimization will be limited at two. For this simulation, the chosen numbers are considered reasonable but may be tuned during further testing.

Results also indicate that the excitation limit is not a very sensitive parameter in this setup. However if the limit is set much lower while the number of stored data is kept the same this will yield more possible key parameters used in optimization. This in turn could quickly increase computational time and may also be more prone to rapid changes without much knowledge about the operating conditions.

During simulation it is observed that 15 updates is performed as data samples become available. Results over the different update intervals is presented in Figure 6.2. The adaptive model comes closer to the mean value of the measurement compared

6. Results

to the baseline . In addition, the RMSE gradually decreases. The cumulative error using the baseline model indicates that the model overestimates powerloss. For the adaptive model the powerloss is still overestimated but to a smaller extent.

Analyzing the results over the entire data set after running the adaptive approach, the adaptive model is shown to have smaller error values compared to the baseline model. For instance, the mean value of powerloss for the ISG in the measurements is 1.20 kW, the baseline model is 1.37 kW and the adaptive model is 1.29 kW. The RMSE value of the adaptive model is 0.45 kW, a decrease of 7.5 % from the RMSE value of 0.49 kW of the baseline model. Average error decreases by 17.7 % from 0.29 kW in the baseline model to 0.24 kW in the adaptive model.

Furthermore the number of unique key parameters was 7 and thus the adaptive map have updated a total of 7 values. An overview of key parameters is presented in Figure 6.3 and a comparison of the baseline model and the adaptive model at the end of the simulation is presented in Figure 6.4.

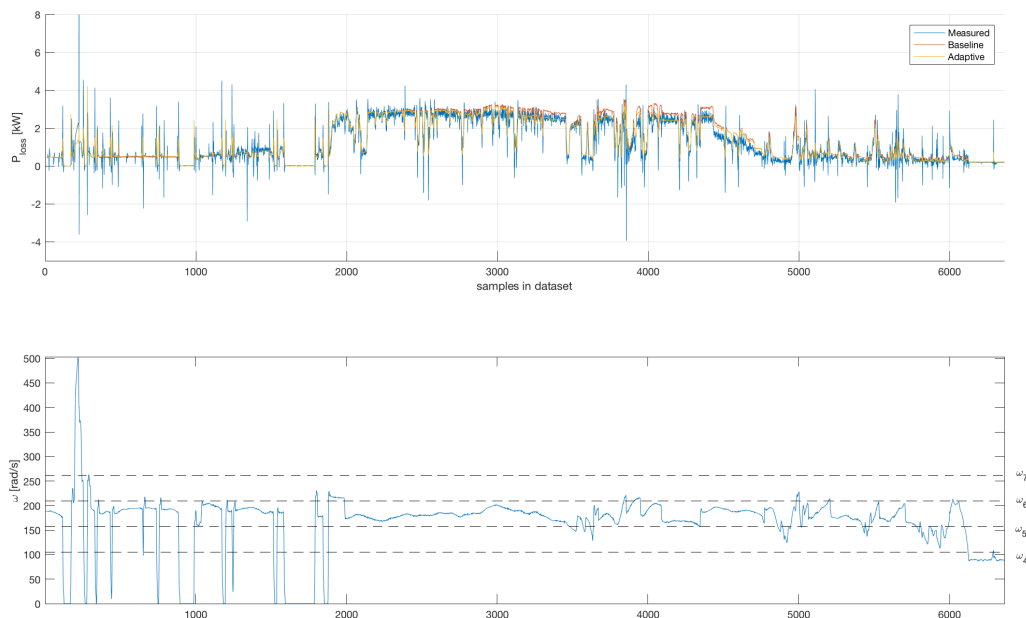


Figure 6.1: Powerlosses in the ISG. Measured values are shown with blue, estimated values using the baseline model are shown in red and estimated values using an adaptive model are shown in yellow. It can be seen that the model error of the adaptive model decreases compared to the baseline model with regards to the measurements.

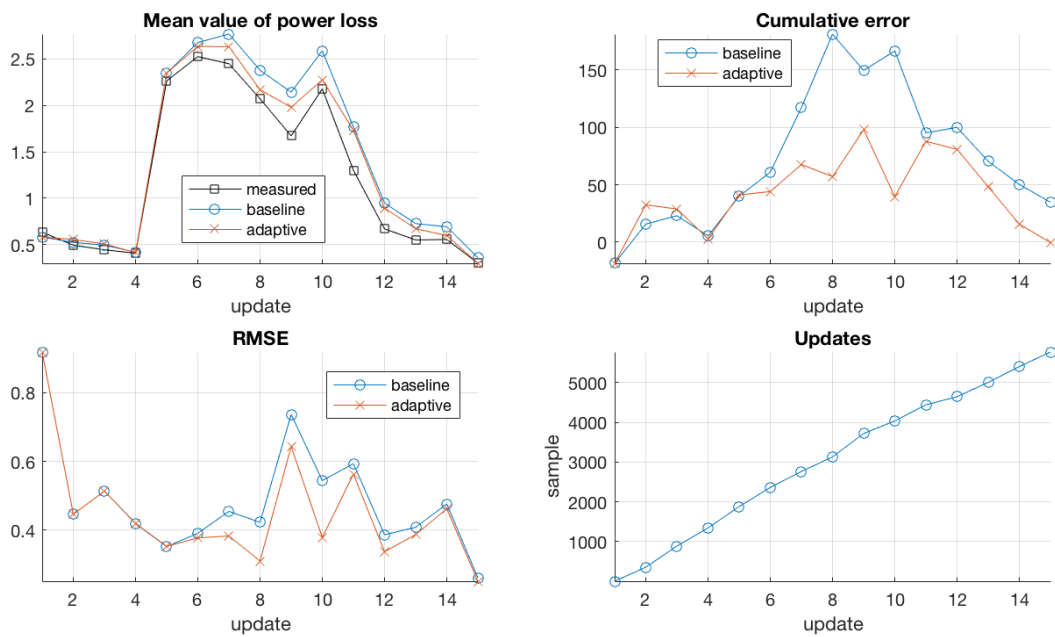


Figure 6.2: Observations from using the adaptive approach over the given data set in the ISG. A total of 15 updates is performed. In the upper left figure it is seen that the adaptive model lies closer to the mean value of the measurement data compared to the baseline model. The upper right picture shows that the cumulative error gradually decreases compared to the baseline model. The bottom left picture shows how the adaptive model have a lower RMSE and the bottom right picture shows at which samples the update was performed.

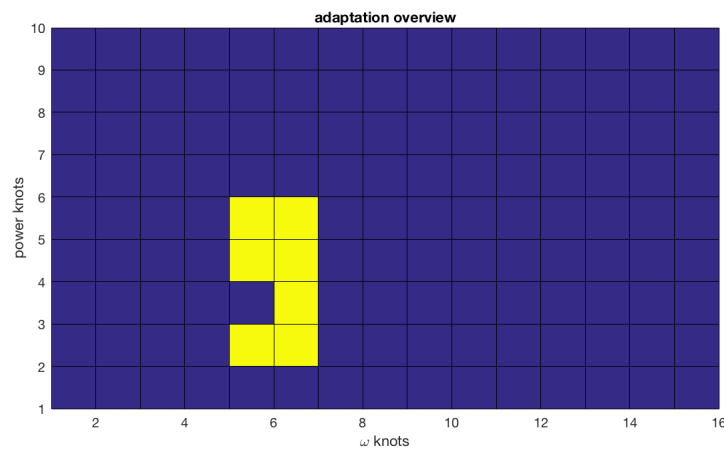


Figure 6.3: Identified key parameters for the ISG over the given data set when using the adaptive approach. Here a total of 7 unique points was used during optimization.

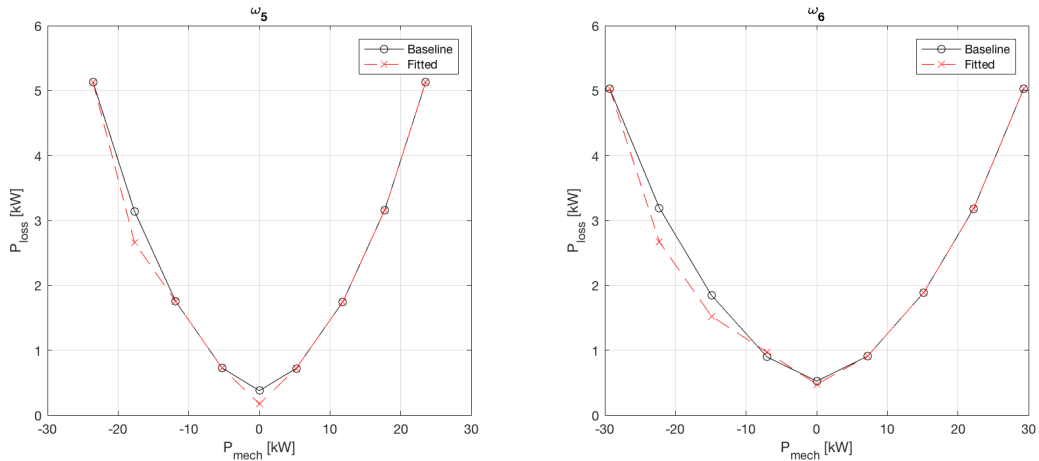


Figure 6.4: Comparison of baseline model and the current model of the ISG after the final update created by performing continuous optimization to minimize model error. The fitted model using the adapted approach is shown in dashed red lines and the baseline model is shown in black.

For the ERAD a data set with $N = 1100$ samples is used to evaluate the model error. Powerlosses over the entire data set and corresponding profile of ω are presented in Figure 6.5. The same number of stored data is used in simulation at 200 samples and again the excitation limit is set to 80 data points.

During simulation of the data it is in this case observed that 6 updates are performed as data samples become available. Results over corresponding update intervals is presented in Figure 6.6. In the first five updates the mean value of the adaptive model is closer to the measurement and the RMSE decreases. The cumulative error indicates that the baseline model underestimates the powerloss while the adaptive model approaches the measurement values. It can also be noted after the fifth update that the previous updates have been in other operating regions as the baseline model and the adaptive model shows the same results. If simulations was run for a longer period this is expected to change as well as more data in the new operating region will be available.

Analyzing the results over the entire data set in the same way as for the ISG the adaptive model again shows smaller error values compared to the baseline model. The mean value of over the measured set is 1.40 kW, while the baseline model estimates has a mean of 1.04 kW and the adaptive model estimates a mean of 1.21 kW. The RMSE value of the adaptive model is 0.85 kW, a decrease of 7.1 % from the RMSE value of 0.91 kW evaluated using the baseline model. Average error decreases by 17.1 % from 0.64 kW in the baseline model to 0.53 kW in the adaptive model.

The number of unique key parameters here is two, again marking that the adaptive map have updated a total of two values. An overview of key parameters is presented in Figure 6.7 and a comparison of the baseline model and the adpative model at the end of the simulation is presented in Figure 6.8.

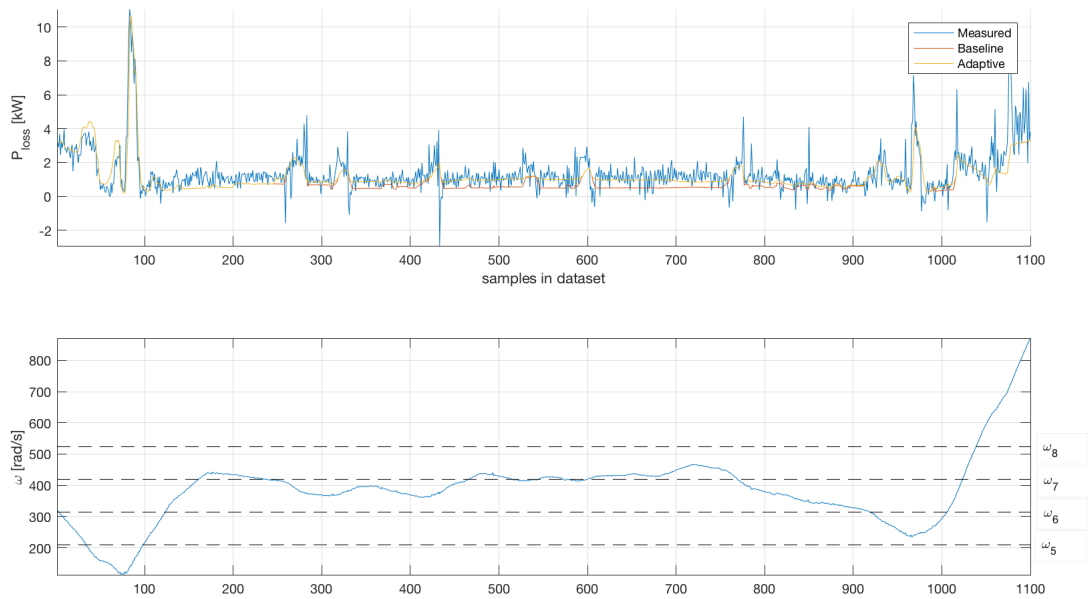


Figure 6.5: Powerlosses in the ERAD. Measured values are shown with blue, estimated values using the baseline model are shown in red and estimated values using an adaptive model are shown in yellow. The model error of the adaptive model decreases compared to the baseline model with regards to the measurements.

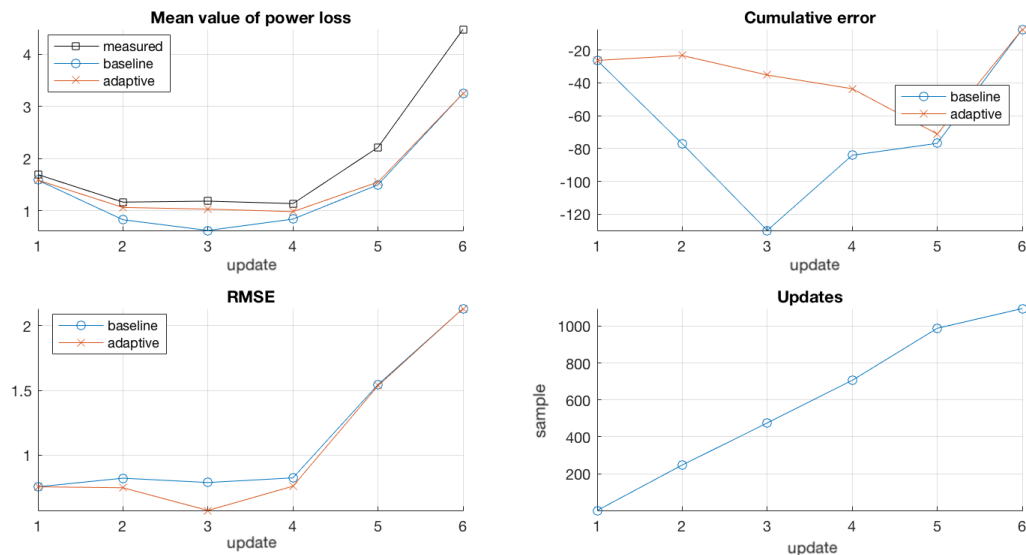


Figure 6.6: Observations from using the adaptive approach over the given data set in the ERAD. A total of six updates is performed. The upper left figure shows the adaptive model is closer to the mean value of the measurement data compared to the baseline model. The upper right picture shows the cumulative error gradually decreasing compared to the baseline model. The bottom left picture shows how the adaptive model have a lower RMSE and the bottom right picture shows at which samples the update was performed.

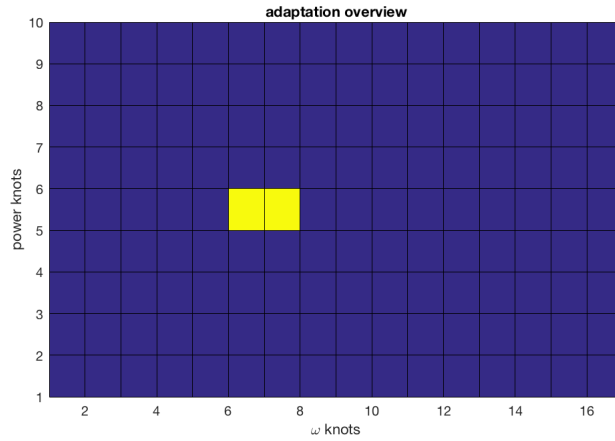


Figure 6.7: Identified key parameters for the ERAD over the given data set when using the adaptive approach. Here a total of two unique points was used during optimization.

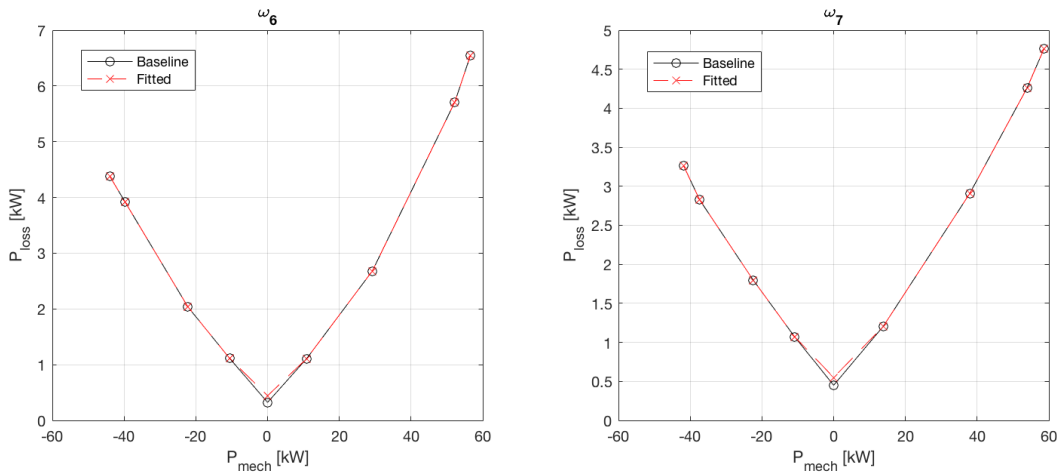


Figure 6.8: Comparison of baseline model and the current model of the ERAD after the final update created by performing continuous optimization to minimize model error. The fitted model using the adapted approach is shown in dashed red lines and the baseline model is shown in black.

6.1.2 Internal combustion engine

A data set with $N = 2500$ samples is used to evaluate the ICE. Powerlosses over the entire data set and corresponding profile of ω are presented in Figure 6.9. As for the electric machines, the number of stored data is set to 200 samples and the excitation limit is set to 80 data points.

Simulation of the data set shows a total of 45 updates and results over the different update intervals are presented in Figure 6.10. In general the mean value, cumulative error and RMSE achieves better values in the adaptive model compared to the baseline. The cumulative error also indicates that both over- and underestimation

is present for both models.

Analyzing the results over the entire data set after running the adaptive approach shows the adaptive model to have smaller error values compared to the baseline model. The mean value of the powerloss in measurements is 61.35 kW, while the adaptive model yields a mean of 66.80 kW compared to the baseline model mean of 61.35 kW. The RMSE value of the adaptive model is 12.15 kW, a decrease of 14 % from the RMSE value of 14.10 kW of the baseline model. Average error decreases by 24.87 % from 10.13 kW in the baseline model to 7.61 kW in the adaptive model.

Furthermore Figure 6.11 depicts the number of unique key parameters as 7, meaning the adaptive model have updated a total of 7 parameters. The parameters are distributed over four different speeds and one to two power points in each speed. A comparison of the baseline model and the adaptive model at the end of the simulation is presented in Figure 6.12.

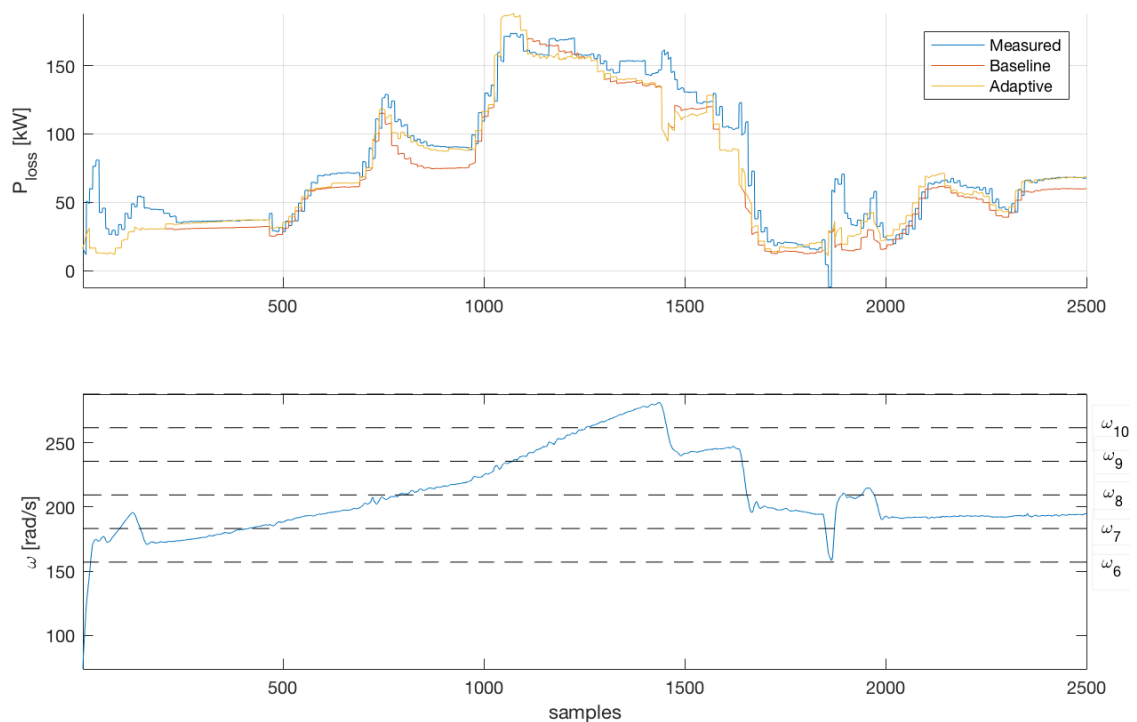


Figure 6.9: Powerlosses in the ICE. Measured values are shown with blue, estimated values using the baseline model are shown in red and estimated values using an adaptive model are shown in yellow. The adaptive model approaches a smaller model error compared to the baseline model as data become available.

6. Results

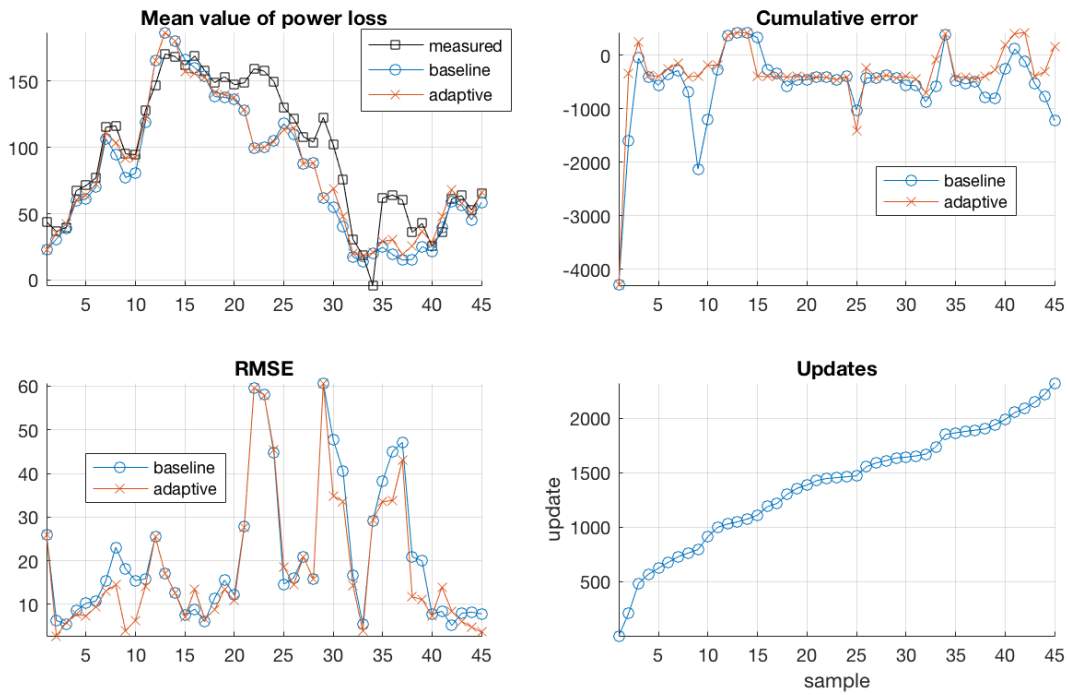


Figure 6.10: Observations from using the adaptive approach over the given data set of the ICE. A total of 45 updates is performed. In the upper left figure it is seen that the adaptive model over most intervals lies closer to the mean value of the measurement data compared to the baseline model. The upper right picture shows that the cumulative error is smaller compared to the baseline model. The bottom left picture shows how the adaptive model has a lower RMSE and the bottom right picture shows at which samples the update was performed.

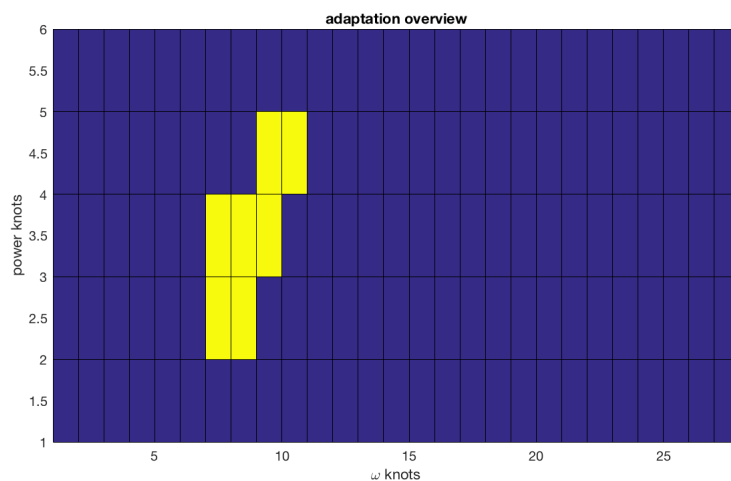


Figure 6.11: Identified key parameters for the ICE over the given data set when using the adaptive approach. A total of 7 unique points was adapted during optimization over four different speeds.

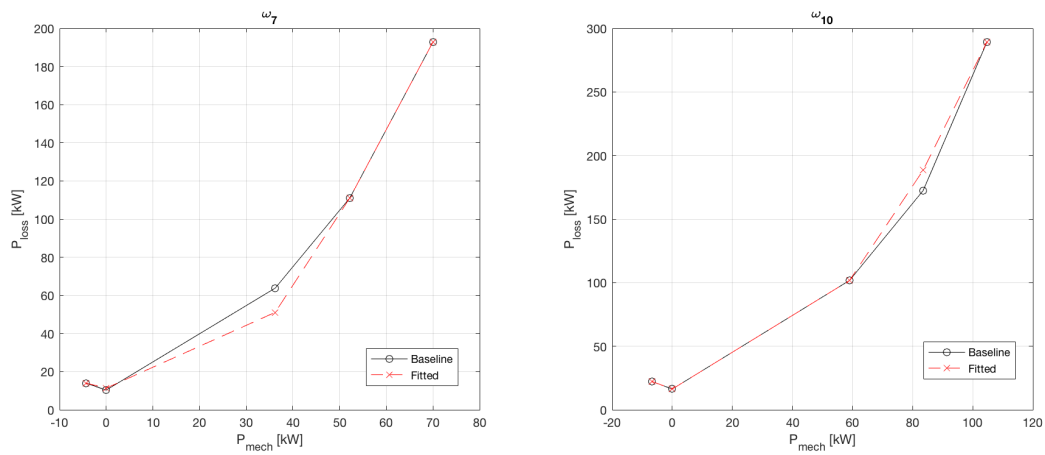
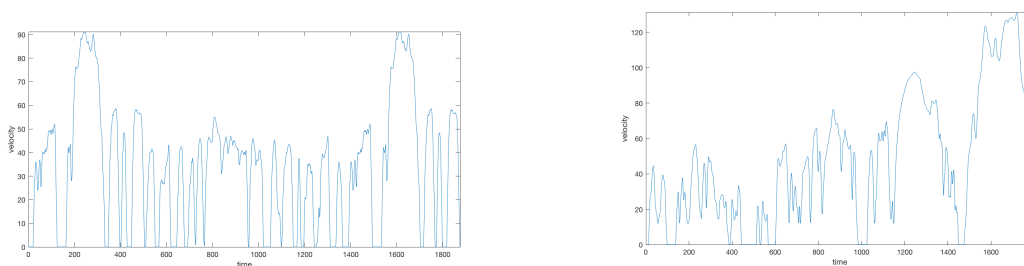


Figure 6.12: Comparison of baseline model and the current model of the ICE after the final update created by performing continuous optimization to minimize model error. The fitted model using the adapted approach is shown in dashed red lines and the baseline model is shown in black.

6.2 Impact on fuel consumption

The system performance is evaluated using two different driving cycles, WLTC and FTP-75, where the adaptive approach is applied together with the ECMS-solver as described in Section 5.3. FTP-75 is a driving cycle which represents urban driving with frequent stops while WLTC [18] is a driving cycle divided into four parts with different average speeds ranging from low, medium, high and extra high. Both cycles are shown in Figure 6.13.



(a) Velocity profile of FTP-75 driving cycle.

(b) Velocity profile of WLTC driving cycle.

Figure 6.13: Driving cycles used for system performance evaluation.

The baseline model used is the same original model for each component while the correct model was derived from measurements to represent the actual vehicle based on observations for corresponding component. Investigating powerloss estimations based on the baseline and correct model for each of the driving cycles, Figure 6.14 and 6.15, shows that there is a larger model error present for the WLTC cycle.

6. Results

Hence there is a bigger room for improvement which also shows in the result as the fuel reduction over the WLTC cycle is more than twice as high compared to the FTP-75 cycle. In both estimations it is observed that the model error is larger for the ICE.

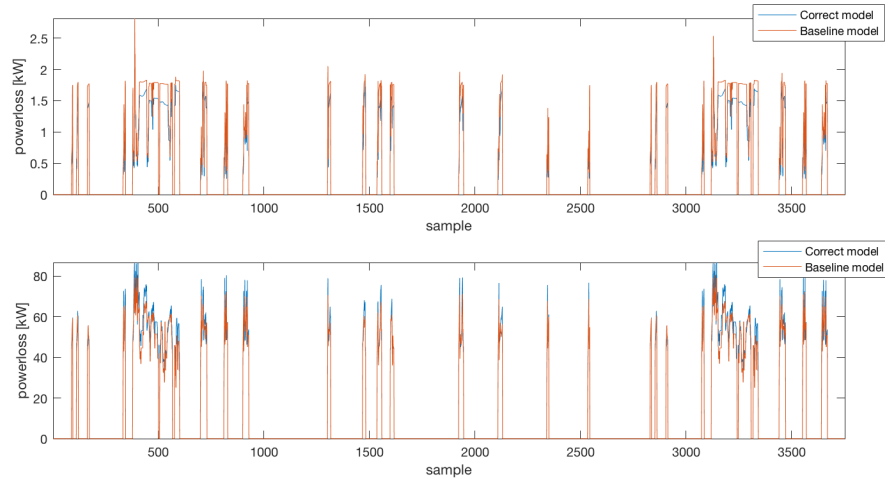


Figure 6.14: Powerloss estimations during the FTP-75 driving cycle using the baseline model and correct model. The upper picture shows powerloss for the ISG while the bottom picture shows powerloss for the ICE.

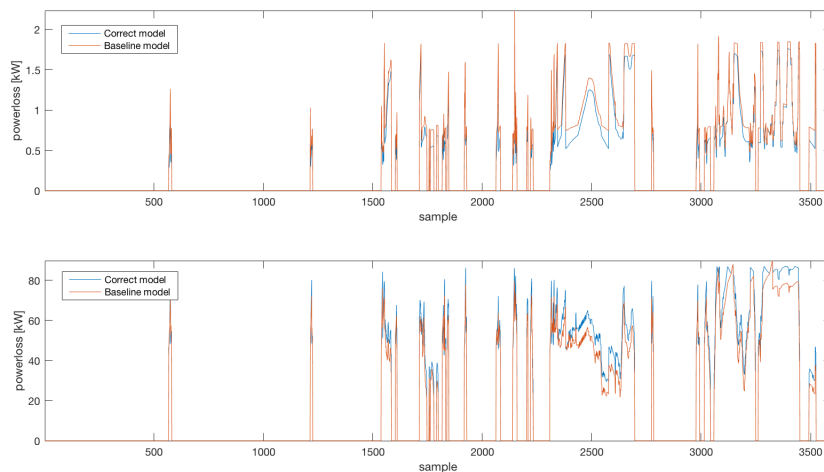


Figure 6.15: Powerloss estimations during the WLTC driving cycle using the baseline model and correct model. The upper picture shows powerloss for the ISG while the bottom picture shows powerloss for the ICE.

Overall the results from simulation presented in Table 6.1 suggest the adaptive approach yields a decrease in the fuel consumption over the both driving cycles while sustaining battery charge, as shown in Figure 6.16-6.17. When taking into consideration the velocity profile and error estimations using the baseline model it is

also suggested that the adaptation have a higher impact during high and extra high velocities.

Table 6.1: Fuel consumption from simulation with a shrinking horizon using different models during ECMS in two different driving cycles.

Cycle	Baseline model	Adaptive model	Change
WLTC	1.25410 kg	1.23650 kg	-1.40 %
FTP-75	0.81495 kg	0.81107 kg	-0.48 %

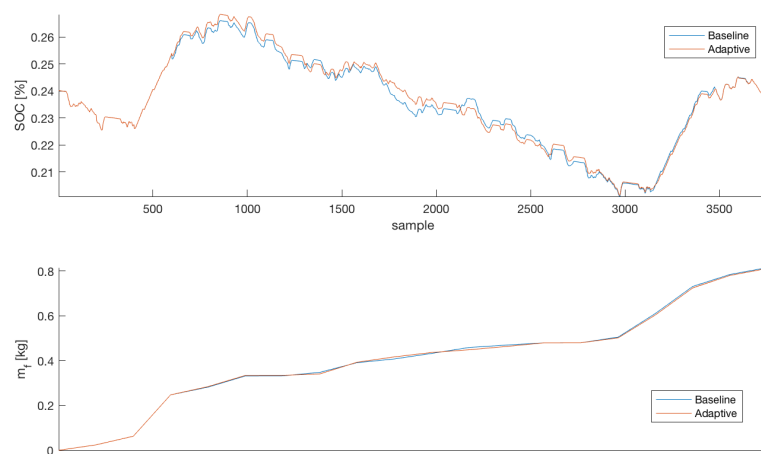


Figure 6.16: State of charge trajectories and fuel consumption of the FTP-75 cycle for simulations using the baseline and adaptive model respectively during ECMS.

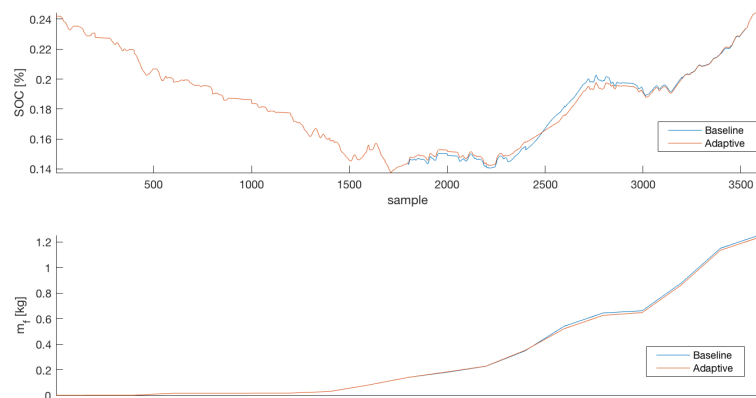


Figure 6.17: State of charge trajectories and fuel consumption of the WLTC cycle for simulations using the baseline and adaptive model respectively during ECMS.

7

Conclusion and Future Work

In this thesis online adaptation of look-up tables containing data for estimating powerlosses during vehicle operation is explored. At first, measurements collected from actual vehicle operation is analyzed and it can be concluded that there is model errors present for all three components in relation to the baseline model. Although the baseline model in many cases exhibits the same behaviour and trends as the measurements, it is shown to be room for improving accuracy of the model. The electric machines, ISG and ERAD, exhibit less model error compared to the engine.

The proposed algorithm uses a clustering approach for handling data and finding key parameters used to perform fitting of the models based on available data. The data fitting is carried out by solving an optimization problem where the objective function is expressed as a trade-off between model error and deviation from the original baseline model. Additionally, the problem can be formulated such that it can be solved using existing solvers. Using the adaptive approach, a better estimation of powerloss compared the baseline model for all three components over a set of given data is obtained while fulfilling the convexity constraints of the models. When integrating the algorithm with an ECMS solver, the simulation results also demonstrates improved fuel consumption over the FTP-75 and WLTC driving cycles. Furthermore it is indicated that the adaptation have a bigger effect during high velocities or a relatively steady state operation as this provides less scattered data. The goal of using online model adaptation is to be able to compensate for model errors, variations and neglected dynamics and the results of this work suggests it may be beneficial to incorporate this in a hybrid electric vehicle.

A straightforward algorithm is proposed, which indicates that it may be relatively simple to achieve a model which adapts to current operating conditions and variations from the baseline model. However, it would certainly be beneficial to explore other algorithms to compare results regarding both accuracy, robustness and efficiency. For instance, a constrained recursive least square method could be of interest.

One of the main advantages with the proposed adaptive approach is that there is no need for new hardware or components, instead this could be implemented with only software modifications. However, for this to be possible the algorithm must be made more efficient to keep up with the information flow within the vehicle. A real-time implementation would also require the memory allocation and storage to be investigated in detail and compared to the achieved accuracy to see if the approach is viable and not too demanding in relation to the end result.

7. Conclusion and Future Work

A possible drawback of using this adaptive approach is that only parameter values within certain operating regions are updated based on where data is located. Therefore the implications of this should be further investigated over the entire model and the other operating regions which are not excited very often during vehicle operation.

Bibliography

- [1] P. Hertzke, N. Müller, S. Schenk, and T. Wu, *The global electric-vehicle market is amped up and on the rise*, <https://www.mckinsey.com/industries/automotive-and-assembly/our-insights/the-global-electric-vehicle-market-is-amped-up-and-on-the-rise>, Accessed: 2018-05-09.
- [2] H. Kaas, “Automotive revolution—perspective towards 2030: How the convergence of disruptive technology-driven trends could transform the auto industry”, *McKinsey & Company*, 2016.
- [3] Volvo Car Group, *Volvo cars to go all electric*, <https://www.media.volvocars.com/global/en-gb/media/pressreleases/210058/volvo-cars-to-go-all-electric>, Accessed: 2018-02-01, Volvo Car Group, 2017.
- [4] S. Onori, L. Serrao, and G. Rizzoni, *Hybrid electric vehicles: energy management strategies*. Springer, 2016.
- [5] A. Sciarretta and L. Guzzella, “Control of hybrid electric vehicles”, *IEEE Control systems*, vol. 27, no. 2, pp. 60–70, 2007.
- [6] J. C. P. Jones and K. R. Muske, “Identification and adaptation of linear look-up table parameters using an efficient recursive least-squares technique”, *ISA transactions*, vol. 48, no. 4, pp. 476–483, 2009.
- [7] M. Vogt, N. Müller, and R. Isermann, “On-line adaptation of grid-based look-up tables using a fast linear regression technique”, *Journal of dynamic systems, measurement, and control*, vol. 126, no. 4, pp. 732–739, 2004.
- [8] E. Höckerdal, E. Frisk, and L. Eriksson, “EKF-based adaptation of look-up tables with an air mass-flow sensor application”, *Control Engineering Practice*, vol. 19, no. 5, pp. 442–453, 2011.
- [9] B. Fridholm, T. Wik, and M. Nilsson, “Kalman filter for adaptive learning of look-up tables with application to automotive battery resistance estimation”, *Control Engineering Practice*, vol. 48, pp. 78–86, 2016.
- [10] C. Guardiola, B. Pla, D. Blanco-Rodriguez, and L. Eriksson, “A computationally efficient Kalman filter based estimator for updating look-up tables applied to NOx estimation in diesel engines”, *Control Engineering Practice*, vol. 21, no. 11, pp. 1455–1468, 2013.
- [11] A. Stotsky, “Adaptive estimation of the engine friction torque”, *European Journal of Control*, vol. 13, no. 6, pp. 618–624, 2007.
- [12] A. Magnani and S. P. Boyd, “Convex piecewise-linear fitting”, *Optimization and Engineering*, vol. 10, no. 1, pp. 1–17, 2009.
- [13] R. Rajamani, *Vehicle dynamics and control*. Springer Science & Business Media, 2011.

- [14] L. Serrao, S. Onori, and G. Rizzoni, “ECMS as a realization of Pontryagin’s minimum principle for HEV control”, in *American Control Conference, 2009. ACC’09.*, IEEE, 2009, pp. 3964–3969.
- [15] H. Ahmadi, J. R. Martí, and A. Moshref, “Piecewise linear approximation of generators cost functions using max-affine functions”, in *Power and Energy Society General Meeting (PES), 2013 IEEE*, IEEE, 2013, pp. 1–5.
- [16] L. Ljung, “System identification”, in *Signal analysis and prediction*, Springer, 1998, pp. 163–173.
- [17] J. Almgren and G. Elingsbo, *Route based optimal control strategy for plug-in hybrid electric vehicles*, 2017.
- [18] ACEA, European Automobile Manufacturers Association, *What is WLTP and how does it work?*, <http://wltpfacts.eu/what-is-wltp-how-will-it-work/>, Accessed: 2018-05-11.